Asperous coordinates regenerative timing by regulating damage-induced WNT Signaling

Si Cave[1], Manashi Sonowal[2], Chloe Van Hazel[1], Petra Fromme[2], Robin E. Harris[1]*

[1]Arizona State University, 427 E Tyler Mall LSE 229, Tempe, AZ 85287-4501

[2]Center for Applied Structural Discovery, Biodesign Institute, Arizona State University, Tempe, Arizona, 85287, United States of America.

*Corresponding Author

Robin Harris: robin.harris@asu.edu

Orchid ID: 0000-0001-6945-6741

Si Cave: sacave@asu.edu

Orchid ID: 0000-0002-0293-7644

Chloe Van Hazel: cvanhaz1@asu.edu

Orchid ID: 0009-0007-6175-2678

Manashi Sonowal: msonowal@asu.edu

Orchid ID: 0000-0002-4665-8831

Petra Fromme: pfromme@asu.edu

Orchid ID: 0000-0003-0953-4909

Summary

Tissue regeneration requires precise control of signaling pathways to direct proliferation, differentiation, and patterning. While early responses to injury are well characterized, how differentiation is coordinated during later stages remains unclear. Here, we identify Asperous (Aspr), an EGF-repeat protein, as a regeneration-specific regulator in *Drosophila* wing discs. Aspr is dispensable for wing development but is strongly induced within 24 hours post-injury. Maintaining *aspr* expression inhibits differentiation and alters reparative growth, while loss impairs regeneration. Structural and expression analyses show Aspr is a membrane-associated extracellular protein secreted in extracellular vesicles (EVs), where it co-localizes with the WNT ligand Wingless (Wg). We find Aspr regulates post-injury but not developmental Wg signaling, potentially by influencing its secretion or availability via EVs. These findings suggest Aspr regulates WNT activity to ensure proper timing of cell fate specification during regeneration, revealing a mechanism by which signaling dynamics are temporally controlled during tissue repair.

Introduction

Tissue regeneration restores lost or damaged structures through coordinated reactivation of growth, differentiation, and patterning programs. Across different species and tissue types, this process frequently reuses developmental signaling pathways, including Wingless/Wnt (WNT), Bone Morphogenetic Protein (BMP), Notch, and JAK/STAT.[1-3] These pathways drive key regenerative processes such as stem cell activation, proliferation, morphogenesis, and repatterning. Among them, WNT signaling is particularly well studied and broadly conserved,[4] playing a pivotal role in regeneration of diverse tissues, including zebrafish fin and CNS,[5-9] mouse and fly intestine,[10-13] and planarian body axis.[14,15] In many contexts, WNT ligands are rapidly induced after injury, activating canonical or non-canonical pathways to promote proliferative expansion.[4,16] Moreover, WNT signaling is also required during the late stages of regeneration to re-establish spatial patterning cues, guiding the reconstruction of discrete tissue identities after proliferative growth.[4,16] However, while the presence and function of WNTs and other pathways during regeneration are well documented, how their activity is precisely timed and regulated across different phases of regeneration remains poorly understood. This becomes critical for regenerating complex tissues through successive stages, which can require events like wound epithelium formation, development of a blastema, proliferative expansion, and tissue differentiation to occur sequentially.[1,17] Each of these phases demand tight temporal control of signaling to maintain the correct progression of events, and understanding the mechanisms that coordinate such transitions remains an important challenge in the field.

The *Drosophila* wing imaginal disc provides an ideal model to dissect regeneration at high resolution, owing to its well-characterized developmental programs, advanced genetic tool kit and substantial ability to regenerate following injury.[18] In addition to its historical use in studying growth and pattern formation,[19] the wing disc has also emerged as a powerful system to identify genetic factors that regulate tissue regeneration.[18,20] To better understand the events of injury induction and gene expression during regeneration, we previously developed a versatile genetic ablation system called DUAL Control.[21,22] This system enables independent induction of cell death alongside spatially and temporally restricted manipulation of gene expression in surrounding tissues, allowing us to interrogate regeneration in a controlled and reproducible manner. Using this approach, we previously identified and characterized several different genetic and epigenetic factors that are required for proper restoration of the wing disc after injury.[22-25]

One such factor is *asperous* (*aspr*), a gene that encodes an extracellular EGF repeat–containing protein that is highly induced in early regenerating tissue. We initially identified *aspr* based on its proximity to a damage-responsive enhancer and its strong transcriptional upregulation following ablation,[22] although its function in regeneration remained unclear. Here we have performed a comprehensive characterization of *aspr*, finding that it is not expressed during normal wing disc development and is dispensable for both viability and wing formation, yet its loss impairs regeneration, suggesting a regeneration-specific role. We show that *aspr* is present only transiently during the early phase of regeneration, and that prolonging its expression disrupts proper regenerative growth and delays the onset of late-stage patterning. Mechanistically, we find that *aspr* interferes with the reactivation of several patterning genes normally induced late in regeneration downstream of *Drosophila Wnt1*, *wingless* (*wg*), indicating *aspr* normally modulates WNT signaling. Further analysis reveals that the Aspr protein is secreted, and associates with extracellular vesicle-like structures, which colocalize with Wg protein explicitly during regeneration, suggesting it could potentially act as an extracellular regulator of WNT ligand distribution or availability in this context. Although vesicle-mediated transport has been proposed as a mechanism for WNT ligand trafficking during development,[26-29] its role in regeneration has not been previously demonstrated. Thus, our work identifies a novel, regeneration-specific modulator of WNT signaling and highlights the critical role of regulating extracellular signaling to precisely coordinate gene expression timing necessary for successful tissue regeneration. Given the conserved role of WNT signaling in regeneration across diverse species,[16] these findings have broad implications for understanding how signaling transitions are coordinated during regeneration.

Results

Damage-induced and developmental *aspr* are regulated by distinct mechanisms

Our previous work to characterize epigenetic and transcriptomic changes associated with regeneration identified *aspr* (previously *CG9572*),[22,25] which RNA-seq showed to be one of the most strongly induced genes in regenerating discs.[25] Other groups have shown that *aspr* is damage-responsive and associated with blastema cells.[30,31] Notably, these studies also show *aspr* is absent from undamaged pouch tissue, suggesting a regeneration-specific role, though this role remains unclear. To better understand its function, we visualized *aspr* expression after damage using HCR fluorescence *in situ* for transcript detection and an anti-Aspr antibody generated for this study. In

undamaged early L3 discs (84 h after egg deposition, AED), *aspr* is expressed in the proximal notum and weakly above the dorsal hinge but is absent from the pouch (Figure 1A). This pattern persists in late L3 (108 h AED, Figure 1F). Unfortunately, the anti-Aspr antibody we developed exhibits low sensitivity and only weakly detects Aspr protein (Figure S1A and S1A'). Therefore, we relied on transcript detection for subsequent analyses. Using the DUAL Control (DC) ablation system[21] to activate JNK-mediated apoptosis via activated *hempiterous* in the distal pouch (DC^{hepCA}), we found *aspr* is upregulated in blastema cells by 12 h after heat shock (AHS), maintained through 18-24 h, and largely absent by 36 h (Figures 1B-E). By contrast, late L3 discs show only weak *aspr* upregulation following ablation (Figure 1G). We also tested necrotic cell death using DC^{gluR1}.[23,24] Similar to apoptosis, necrosis triggers *aspr* induction around the wound in early L3, peaking at 18 h and diminishing by 36 h (Figures 1H and 1I). Notably however, necrosis causes *aspr* to occur with a more punctate, potentially nuclear, appearance (Figure 1H), likely reflecting the distinct responses to necrotic injury we previously characterized.[23,24] Late L3 discs showed minimal *aspr* expression post-necrosis (Figure 1J).

Beyond genetic injury, *aspr* is also expressed in neoplastic tumors (*sd>lglRNAi*, Figure S1B-D) and early after physical wounding (Figure S1E), supporting its role as a generalized early stress-response gene. Similarly, in other imaginal discs (leg, haltere, eye), *aspr* is mostly undetectable in undamaged tissue and becomes induced upon ablation (Figures S1F-H). As with many genes involved in regeneration, *aspr* appears to be regulated by a Damage-Responsive, Maturity-Silenced (DRMS) enhancer, a class of regulatory elements that are activated by JNK and JAK/STAT signaling but epigenetically silenced in mature discs.[22,25,32] We previously identified a DRMS enhancer upstream of *aspr* that becomes accessible after damage in early L3 but not late L3 discs.[22] A reporter for this region (*$DRMS^{aspr}$-GFP*) contains AP-1 and Stat92E binding sites (Figure S1I), overlaps with JNK activity (*AP-1-RFP*, Figures 1K and 1L), and mirrors *aspr* expression in early L3, while being only weakly active in late L3 (Figures 1M and 1N). This behavior is consistent with the DRMS regulating *aspr* via JNK in the context of damage. Since regenerative ability varies across the disc,[33] we explored the regionality of $DRMS^{aspr}$ activity by ablating tissue along the anterior/posterior (A/P) boundary using *ptc>hep^{CA}* or *ptc>egr*. This domain includes the notum, hinge, and pouch (Figure 1O and 1O'), all of which activate JNK after damage.[33] While only the pouch typically activates regeneration-associated genes, *aspr* is induced along the full stripe in early L3 discs (Figures 1P and 1P'), including non-regenerating notum tissue. In late L3, *aspr* is only induced outside the pouch (Figure 1Q'), but the *$DRMS^{aspr}$-GFP*

reporter is entirely inactive (Figure 1Q). Thus, damage-induce *aspr* is likely regulated by the DRMS^{aspr} in the regeneration-capable pouch, while damage-responsive enhancers that are not silenced with maturity likely drive *aspr* expression outside of this region.

Interestingly, we noted that developmental *aspr* expression in the notum overlaps with JNK activity that is required for thorax closure during pupariation (Figure 1K).[34] In *hep* mutants, damage-induced *aspr* is diminished, while developmental expression persists (Figure 1R). Similarly, expression of a dominant-negative JNK in the notum (*pnr>hep^{DN}*) fails to suppress *aspr* in the notum (Figures 1S and 1T). Since the DRMS^{aspr} reporter is inactive in the notum of undamaged discs (Figure 1M), together these observations suggest that developmental and regenerative *aspr* are regulated by distinct mechanisms.

Loss of *aspr* blocks regeneration but does not affect normal development of the wing disc

As *aspr* is strongly upregulated after injury but shows limited developmental expression, we tested whether its removal affected either context. The DC system allows heat shock-induced, flip-out-mediated expression of UAS-transgenes specifically in the pouch, driven by *DVE>>GAL4* during and after damage.[21] Two RNAi constructs effectively knock down *aspr* in the pouch, reducing its damage-induced expression (Figures 2A and 2B). We found a third RNAi line (*TRiP.HMJ22471*) was ineffective and did not use it further. The knockdown of *aspr* in undamaged discs has no visible effect on wing development (Figure 2C), consistent with its minimal expression in normally developing discs (Figure 1A). However, knockdown during regeneration significantly impairs recovery in both early and late L3, shown by wing scoring (Figure 2E) and adult wing area (Figure 2F). The loss of *aspr* does not alter damage-induced JNK signaling (*Mmp1* expression, Figures 2G and 2H) or cell death caused by DC^{hepCA} ablation, supporting its activity being downstream of JNK. Beyond these observations, the knockdown of *aspr* does not immediately indicate its function, though it is clearly essential for regeneration and dispensable for normal development.

To confirm this, we tested the *aspr^{MI02471}* allele, a *Mi[MIC]* insertion that likely represents a transcriptional null.[22] HCR *in situ* confirms that hemizygous males and homozygous females lacked detectable *aspr* transcripts in the wing disc, both in undamaged and damaged conditions (Figures 2I and 2J). These mutants displayed no overt developmental phenotypes, including in wing patterning or size (Figure 2K). Moreover, while *aspr* is normally

expressed in the notum, where JNK and other signals govern thoracic patterning and bristle formation, these structures were unaffected in mutants (Figure 2L). We did observe a modest but significant developmental delay in *aspr*^{MI02471} larvae, which is more pronounced in homozygous females (Figures S2A and S2C). This delay is not seen with RNAi knockdown in the wing (Figure S2B), suggesting there is either a role for *aspr* in developmental timing outside of the wing, or an unrelated mutation in the *Mi[MIC]* line. Importantly, as in knockdown experiments, *aspr*^{MI02471} mutants showed reduced regenerative capacity in both early and late L3 discs (Figure 2M). Thus, although the specific function of *aspr* remains unclear, these data confirm that it is required for regeneration but not for normal development.

Maintaining *aspr* expression impacts repatterning during regeneration

aspr is normally upregulated only during the first 24 h of repair (Figures 1A-1E), and while loss-of-function analyses show it is required for regeneration, they do not clarify its role. Since *aspr* is dispensable for normal development but essential for early regeneration (Figure 2), we investigated its function via ectopic expression. We previously used a UAS-driven multi-tagged construct (*UAS-aspr-FLAG.3xHA*) to perform preliminary investigations of its effects,[22] but this causes ectopic vein tissue in undamaged discs, a phenotype that is not seen with the untagged version we generated (*UAS-aspr*) (Figures S3A and S3B). Additionally, the multi-tagged construct showed inconsistent transcript levels in discs (Figure S3C). To ensure reliable findings, we generated a new single HA-tagged transgene (*UAS-aspr-HA*) and expressed it using both non-ablating (DC^{NA}) and ablating (DC^{hepCA}) versions of DUAL Control. Expression of the untagged and single tagged was confirmed by HCR and/or anti-HA staining (Figures 3A, 3B, S3D and S3E). Strikingly, we found that Aspr protein occurs with two distinct appearances: “cellular Aspr,” associated with apical membranes, and “punctate Aspr,” found as discrete foci at or above the apical surface (Figure 3A’ and Figure 7G-J). This appearance was seen when expressed in the notum, hinge and pouch regions of the disc (Figure 3B and 3B’), but was not observed with the FLAG.3xHA multiple-tagged construct (Figure S3F). Despite these distinct appearances, ectopic Aspr expression during development in the pouch (*DVE>>GAL4*), or throughout the entire anterior or posterior disc (*ci-GAL4* or *hh-GAL4*) had no visible effects on disc proliferation, signaling pathways, or gene expression (Figures 3C-H, S8A-C and S8O), nor did it affect adult wing patterning or size (Figures 3I-K and

S3G and S3H). This held true for both the single HA-tagged and untagged constructs (Figure S3B), reinforcing that *aspr* lacks a developmental role even when ectopically expressed.

We next examined its function during regeneration. Although endogenous *aspr* is normally downregulated after 24 h (Figures 1A-1E),[31] continuous expression of *aspr-HA* (or untagged *aspr*) throughout regeneration impaired recovery in both early and late L3 discs (Figures 3L, 3N, S3I and S3J). To determine whether this was due to the higher level of Aspr in early regeneration or its inappropriate presence in late regeneration, we used GAL80^{ts} to restrict *aspr-HA* expression to either the first 24 h AHS, or from 24 h AHS onward. Early expression had no effect (Figures 3M and 3P), while late expression significantly impaired regeneration (Figures 3M and 3Q). This suggests that while Aspr is normally required early, and ectopic Aspr at this stage has no effect, its persistence beyond 24 h disrupts recovery.

When Aspr is maintained in late regeneration, in addition to reduced regeneration we also observed a distinct “box wing” phenotype in a subset of adults (Figures 3N, 3O, 3R and 3R’): ~38% in early L3 and 5% in late L3 (Figure 3O). These wings showed consistent features that predominantly affect the anterior wing (Figures 3R and 3R’), including 1) reduced intervein 2 (I2) between longitudinal veins 2 and 3 (LV2, LV3), 2) ectopic veins along LV2 and LV3, 3) loss of anterior wing margin bristles, 4) variable loss of ACV and PCV, and 5) a squared-off wing blade. These phenotypes also occurred with the untagged transgene in ablated wings (Figure S3K). However, these features were absent when *aspr-HA* was expressed in undamaged wings (Figures 3I and 3J) or when expression was restricted to early regeneration (Figure 3P). These findings indicate that mis-patterning arises from prolonged Aspr expression. Since loss-of-function studies do not clearly reveal its specific role (Figure 2D), we focused on these phenotypes to better understand the function of Aspr in regeneration.

Aspr affects regrowth of the anterior compartment

To better understand the "box wing" phenotype resulting from *aspr* expression in late regeneration, we measured the regions of the adult wing. Posterior wing area was nearly equivalent to that of ablated wild-type controls, with only a slight reduction (Figure 4A’), whereas the anterior was significantly reduced, accounting for the majority of loss in wing size (Figure 4A). This reduction reflects smaller anterior intervein regions, most significantly of the I2 area (Figure 4B, 4B’ and 4C). I3 and I4 were only measured when the ACV was present. To confirm that *aspr*

affects anterior patterning and growth, we drove *aspr-HA* in solely the anterior or posterior compartments using *ci-GAL4* or *hh-GAL4*. Anterior-specific expression during regeneration produced phenotypes resembling those of whole-pouch expression: I2 reduction, LV2–LV3 fusion and thickening, ectopic vein tissue, ACV loss, and absent anterior margin bristles (Figure 4D). Posterior-specific expression caused only a small reduction in the I6 area (Figure 4E), matching the mild posterior reduction observed in whole-pouch expression (Figure 4A'), but shows no other patterning defects. Expression with either driver in undamaged discs caused no wing phenotypes (Figure S3G and S3H). Thus, the overall box wing phenotype likely reflects a combination of the significant anterior and mild posterior effects (Figure 4D and 4E). Together, these findings strongly suggest that maintaining *aspr* specifically disrupts anterior growth and patterning during regeneration.

To examine the origin of these phenotypes, we monitored regeneration over time with *aspr-HA* expression and stained for *nub*, *ci*, and HA to mark the pouch, anterior compartment, and Aspr, respectively (Figure 4F). The anterior pouch is consistently undergrown from 12–60 h AHS, while the posterior regenerated similarly to controls. Quantification confirmed this observation, with significant anterior undergrowth at all time points except 24 h (Figure 4H and 4I). This aligns with the idea that persistent Aspr only disrupts late regeneration, when endogenous *aspr* is normally downregulated. Ectopic *aspr* without damage has no effect on pouch size (Figures 4G, S4A and S4B), consistent with the absence of adult phenotypes (Figure 3I). To explore this anterior-specific effect, we examined Aspr localization. Although *aspr-HA* transcripts are equally expressed in both compartments (Figure 4J and 4J'), Aspr-HA protein appeared weaker in the anterior pouch of ablated discs (Figure 4K), which could indicate compartment-specific protein localization, stability or usage. We ruled out differences in ablation efficiency, as the *salm* enhancer drives similarly in both compartments (Figure 4L). These results indicate that maintaining Aspr beyond its normal early timing limits regrowth specifically in the anterior pouch. While the reason for this compartment-specificity remains unclear, these data suggest that the normal role of Aspr is to support early regenerative growth in the wing pouch.

Aspr functions to regulate regeneration-specific pouch growth through *vestigial*

To better understand the growth phenotype associated with Aspr during regeneration, we used an E2F reporter (*PCNA-GFP*) to monitor proliferation over time, with Ci staining to mark compartment boundaries. In control discs,

injury triggers strong proliferation near the wound, indicative of a regeneration blastema (Figure 5A). This proliferation peaks at 24-48 h and returns to surrounding levels by 60 h (Figures 5A-5A''' and 5C). We noted that proliferation seems biased toward the anterior, consistent with previous reports showing differences in proliferative potential between compartments.[35-37] Ectopic *aspr-HA* expression reduces proliferation in both compartments, particularly in the anterior (Figure 5B-5B''' and 5C), matching the undergrowth seen in discs and adult wings (Figures 4F and 4H). *aspr-HA* had no effect on proliferation in undamaged discs (Figures 3G and 3H). We attempted to repeat these experiments with anti-PH3 and EdU incorporation, but neither was able to clearly demonstrate these differences (Figures S5A–S5L).

We next screened candidate regulators of growth that might participate in regeneration, and found that *vestigial (vg)*, a key wing selector gene, was disrupted upon *aspr* misexpression. *vg* is normally expressed along the D/V boundary (Figure 5D), and is patterned by *wg*, *notch*, *dpp*, and autoregulation.[38-41] After DC^{hepCA} ablation, Vg is reduced until 36 h AHS but restored by 48 h (Figures 5E-5E''). However, with sustained *aspr-HA* expression, Vg fails to reestablish in the anterior pouch through 60 h AHS and often remains absent until pupariation (Figures 5H-5H''). Interestingly, the *vg* quadrant enhancer (vg^{QE}), which initiates *vg* expression in response to Wg,[38] also shows anterior-specific loss after damage, typically recovering by 48 h AHS in controls (Figures 5F-5G' and S5M-T). Due to genetic constraints, we could not assess vg^{QE} reporter activity in *aspr-HA*-expressing discs, but these results suggest that anterior *vg* is less robustly reinitiated after injury and thus may be more sensitive to prolonged Aspr expression. Together, these data indicate that Aspr maintained in late-stage repair impairs anterior growth by preventing *vg* reactivation during regeneration.

Although anterior pouch tissue is reduced, it still acquires vein/intervein identity (Figures 3R and R'). To assess patterning, we examined *blistered (bs/DSRF)*, which represses vein fate to define intervein regions.[42,43] In undamaged discs, the vein/intervein regions are defined by *bs* expression at 36 h AHS and is unchanged at 60 h AHS (Figures 5I and 5L). After damage, *bs* is transiently lost but returns by 48-60 h AHS (Figures 5J and 5M). *aspr-HA* expression has no clear effect through 36 h (Figure 5K), but by 60 h, I2 fails to form and LV2 and LV3 are fused (Figures 5N-5S), mirroring adult wing defects. Since most of the pouch retains proper *bs* expression despite overlapping Aspr (Figures 5K and 5N), this patterning defect likely results indirectly from impaired growth. Alternatively, as *vg* has been shown to regulate *bs,*[39] the phenotype may stem from disrupted *vg* expression.

Altogether, these findings suggest that Aspr normally promotes proportional growth during early regeneration, partly by supporting timely *vg* reactivation, and when mis-regulated it impairs both regenerative growth and patterning.

Aspr limits expression of late-acting differentiation-associated genes specifically during regeneration

Changes in Vg may account for anterior pouch size reduction and vein/intervein patterning defects in the box wing phenotype, but significant margin abnormalities and loss of bristles is also observed (Figures 3R and 3R'). To investigate this, we examined genes involved in margin cell differentiation. Bristles at the wing margin derive from sensory organ precursors specified by Notch and Wg signaling.[44] Previously, we showed that *aspr* may affect expression timing of the Notch and Wg target gene *cut* (*ct*) at the margin specifically following injury (Figure 6A).[22] We revisited this by testing *aspr-HA* expression during regeneration. Normally, Ct is lost following ablation and restored in all discs by 60 h AHS (Figures 6B and 6C). With *aspr-HA* expression, Ct is fully restored in only 18% of discs (n = 50), with most showing only partial recovery (Figure 6D). *aspr-HA* had no effect on Ct in undamaged discs (Figure S6A), confirming it interferes with *ct* reactivation during regeneration. *ct* is maintained indirectly by Wg via the Notch ligands Delta and Serrate (Figure S6F).[45] Delta expression, normally restored by 60 h AHS (Figure 6E and 6F), is also suppressed by *aspr-HA* (Figure 6G), which may explain the persistent loss of Ct. As both *vg* and *Delta* (and thus indirectly *ct*) are targets of Wg, we examined other differentiation-associated Wg-responsive genes. *aristaless* (*al*) and *Distalless* (*Dll*) encode homeobox transcription factors downstream of Wg.[46] While *Dll* expression was unaffected, Al failed to be restored with *aspr-HA* by 60 h AHS (Figure 6L-6N). Similarly, *achaete* (*ac*), a Wg-responsive factor that promotes neural fate,[47,48] is normally reestablished between 48-60 h AHS (83.9% of discs, Figure 6H-6J), but is absent in most *aspr-HA*-expressing discs (7.9%) (Figure 6K). This likely underlies the reduced bristle counts observed in wings (Figure S6E). These findings indicate that prolonged *aspr* disrupts the reactivation of multiple differentiation-promoting genes (Figure 6O), all of which are directly or indirectly downstream of Wg signaling. None of these genes were altered by *aspr-HA* expression in undamaged discs (Figures S6A-S6D). Many Wg targets also depend on Dpp. However, expression of a *Dpp-lacZ* reporter, pMad, and its target *spalt* (*salm*) were unaffected by *aspr-HA* during development or regeneration (Figures 6L-6N and S6G–S6L). Given the strong overlap between *wg* and *aspr* expression in the blastema,[31] and the fact that several affected genes lie downstream of Wg,

we hypothesize that Aspr normally delays Wg-driven differentiation and sustains early regenerative growth through *vg*.

The idea that Aspr acts to delay differentiation is supported by previous work showing that *aspr* is downstream of the ETS transcription factor Ets21C, which promotes regeneration by supporting the expression of genes like *Mmp1*, *upd3*, *pvf1*, and *aspr*, while preventing premature induction of repatterning genes like *rotund* and *nubbin*.[31] As with *aspr*, mutation of *Ets21C* causes defective, undersized wings post-ablation, but does not affect development. Knockdown of *Ets21C* in ablated wings shows this phenotype (Figures 6P and 6R), but this is almost entirely rescued by co-expression of *aspr-HA* (Figures 6Q and 6R), suggesting that a key function of Ets21C in regeneration is the activation of *aspr* to prevent premature differentiation and promote tissue repair.

Aspr protein structure suggests a role in protein trafficking and secretion

Aspr appears to regulate growth and differentiation during regeneration, but its molecular function remains unclear. To investigate this, we analyzed its predicted protein structure using AlphaFold (Figure 7A and S7A), which reveals a solenoid-like fold with multiple epidermal growth factor (EGF)-like domains (Figure 7B). InterProScan and SMART predict seven EGF domains, while Prosite identifies four. These domains are typical of secreted or membrane-associated proteins involved in signaling, adhesion, and matrix organization[49], supporting a potential extracellular role for Aspr. To further test this, we used six localization prediction tools. Four of these (SignalP, Phobius, Protter, Deeploc) predict a cleavable N-terminal signal peptide with a high-confidence cleavage site between Gly23 and Lys24 (Figures 7C and S7B-E). TargetP and TMHMM also supported this with moderate confidence (~0.5) (Figures 7C, S7F and S7G). These tools also consistently predict Aspr to be extracellular (Figure 7C) reinforcing the idea it is likely secreted. Homology searches identify several structurally related extracellular proteins: human NELL2, human/mouse EDIL3, and *Drosophila* Dumpy (Figure 7D). Alignments of their signal peptides with that of Aspr revealed shared biochemical properties and α-helical structures typical of signal sequences (Figure 7D and S7H-S7L), while RMSD comparisons showed strong similarity to Dumpy (0.189), NELL2 (0.248), mouse EDIL3 (0.635), and human EDIL3 (1.04) (Figure 7E), supporting the idea that Aspr has structural conservation with other secreted

proteins. Together, these structural analyses are consistent with Aspr functioning as a secreted or membrane-associated extracellular protein.

We experimentally tested Aspr secretion using western blots on hemolymph bled from larvae expressing *aspr-HA* (*ci-GAL4>UAS-aspr-HA*). HA was detected in both filtered hemolymph and larval debris (Figure 7F, lanes 8-9), confirming previously published proteomic analysis that identified Aspr in hemolymph[50]. We further processed the filtered hemolymph by subjecting it to additional high-speed centrifugation, which separates extracellular proteins and structures like vesicles away from cells and larger debris. Repeating HA detection on this sample shows that Aspr is present in the supernatant (Figure 7F, lane 4-5), confirming its extracellular nature. Control larvae (w^{1118}) lacked HA signal (Figure 7F, lanes 2-3, 6-7), while anti-Actin was used to indicate cellular presence in each sample (trace Actin in filtrates likely reflects cells such as hemocytes). Together, these findings strongly support Aspr as a secreted extracellular protein.

To validate the localization of Aspr *in vivo*, we re-examined its distribution in the wing disc, focusing on the punctate structures previously observed (Figures 3A and 3B). High-resolution imaging of *ci-GAL4>aspr-HA* discs revealed spherical extracellular vesicle (EV)-like structures (0.1–1 µm) located above the apical surface (Figure 7G), confirmed by co-staining with the apical marker Dlg in transverse sections (Figure 7G'). Although our anti-Aspr antibody has limited sensitivity, we successfully detected EVs using this antibody in *aspr-HA*-expressing discs (Figure S8A-S8B'), ruling out artifacts of HA staining. This was further validated using different anti-HA antibodies and control staining conditions (Figure S8C and S8C'). Most importantly, we also detected EVs using the anti-Aspr antibody in ablated discs expressing only endogenous *aspr*, without ectopic *aspr-HA* (Figure S8D-S8D''). These EVs were smaller (<0.1 µm), more uniform in size, and less frequent, suggesting that ectopic overexpression increases EV size and abundance. Nonetheless, these findings confirm the presence of Aspr-containing EVs under physiological conditions.

Aspr-associated EVs appear alongside intracellular Aspr, which is enriched apically in disc cells (Figure 7G'). An extracellular-optimized staining protocol using non-permeabilized discs eliminates the intracellular Aspr signal, allowing clearer visualization of EVs outside the cells (Figure 7J and J'), located between the disc proper and the overlying peripodial membrane (Figures 7H-7H''). These EVs form in the pouch, hinge, and notum when *aspr-HA* is expressed throughout the anterior compartment via *ci-GAL4*, but are most frequently observed in the pouch (Figures

7G, 7H and 7H'), and can also be detected in other imaginal discs like the leg (Figure S8E). Notably, EVs are present in both undamaged and regenerating discs expressing *aspr-HA* (Figure 7H-7I'). However, regenerating discs show a significantly greater number of the smaller EVs, including in regions lacking active *aspr-HA* expression (Figure 7I and 7I'), suggesting that extracellular Aspr can translocate across the disc specifically during repair. These EVs are distinct from the cellular debris generated by ablation (Figure S8H-S8J'). Overall, these structural, computational, and biochemical results demonstrate that Aspr is a secreted protein, and that it forms EVs in the wing disc, particularly during regeneration, consistent with its proposed role in extracellular signaling.

Aspr co-localizes with Wg and regulates WNT signaling

Maintaining *aspr* expression into late regeneration affects growth and patterning in ways consistent with altered Wg signaling (Figures 5 and 6). Given the predicted protein structure and localization of Aspr to secreted EVs (Figure 7), we tested whether Aspr influences Wg signaling via an extracellular mechanism. Wg is secreted and signals through tightly regulated processes involving chaperones,[51] lipoprotein particles,[52] cytonemes[53,54] juxtracrine mechanisms,[55] and via extracellular vesicles.[26,29,56,57] To examine Wg regulation by Aspr, we expressed *aspr-HA* during development and regeneration while staining for Wg. In undamaged discs, *aspr-HA* has no effect on Wg levels (Figures S9A-S9C). In regenerating discs, however, Wg protein appears somewhat elevated from 18-48 h AHS, especially in the anterior pouch (Figures 8A-D). This is despite *aspr-HA* being driven throughout the pouch. By 60 h AHS, Wg returns to a wild type-like pattern but often appeared distorted at the A/P boundary (Figure 8E), which we hypothesize could be due to misaligned compartments resulting from asymmetric growth (Figure 3). A similar elevation of Wg in the anterior and margin distortion occurs when *aspr-HA* is expressed only in the anterior (Figure S9D-S9H). These findings suggest that *aspr-HA* affects Wg during regeneration; however, Wg levels appear elevated rather than reduced, which is unexpected given the failure to reestablish multiple Wg target genes (*vg, Delta, ct, ac, al*) in the presence of Aspr-HA (Figures 5 and 6). Wg signaling relies on proper cell polarity: one model shows the ligand is produced at the apical surface, then trafficked basally where it activates signaling via receptor engagement.[58,59] Given that Aspr localizes to the apical membrane and within EVs above this surface (Figure 7), we hypothesize that Aspr may sequester Wg at the apical side, restricting its transcytosis to the basal compartment and thereby reducing signaling.

If this model is correct, then activating Wg signaling downstream of the receptor should rescue the reestablishment of Wg target genes caused by sustained Aspr. To test this, we activated Wg signaling downstream of the receptor using three manipulations: knockdown of *Axin* (*Axn*) or *shaggy* (*sgg*), or overexpression of *disheveled* (*dsh*). We assessed expression of the Wg target *ac* as a readout. Normally, *ac* is restored in nearly all regenerating discs at 60 h AHS (Figure 8F) but is blocked by *aspr-HA* (Figure 8G). However, the activation of Wg signaling by any of the three manipulations fully rescues *ac* at 60 h AHS despite persistent *aspr-HA* expression (Figures 8H-8J and 8L), confirming that Aspr can regulate Wg signaling at the level of the Wg ligand or receptor. Each manipulation alone also increases *ac* expression in both undamaged and regenerating discs (Figures S9I-S8N), with particularly strong effects when *dsh* is overexpressed (Figures S9J and S9M). *aspr-HA* mildly reduces these effects in undamaged discs (Figures S9O-S9R), suggesting that Aspr can temper ectopic Wg signaling to some degree even in the absence of injury. Importantly, these rescue experiments also significantly reduce the incidence of the “box wing” phenotype in regenerated wings (Figure 8K) and improves overall regenerative outcomes (Figure 8M). These manipulations, particularly the stronger *Dsh* overexpression and *sgg* knockdown, also result in a phenotype characterized by malformation and ectopic bristles within the wing blade (Figures 8M-8O, S9S and S9T), suggesting these manipulations can go beyond rescuing the suppressive effects of *aspr-HA*, resulting in an “ectopic WNT” phenotype.

These experiments are performed in the context of ectopic *aspr-HA* expression. To confirm that Wg signaling is regulated by Aspr under endogenous conditions, we knocked down *aspr* during regeneration and examined *vg*, a Wg target we know to be affected by Aspr (Figure 3G). Using vg^{QE} activity as a readout, which is typically not restored in the anterior pouch by 36 h AHS (Figure 8P), we found that *aspr* knockdown enables premature reactivation of vg^{QE} (Figure 8Q), supporting the idea that Aspr delays *vg* re-initiation by Wg. Knockdown of *Axn* or *sgg* phenocopies this early activation (Figures 8R and 8S), reinforcing the role of Aspr in modulating Wg signaling. No effects to vg^{QE} were observed in development (Figure S9U-S9X). Finally, we asked whether Aspr and Wg physically colocalize during regeneration. The anti-Aspr antibody was too weak to detect endogenous co-localization with Wg, and thus we examined Wg in *aspr-HA* expressing discs. In undamaged discs, even with optimized extracellular detection of Wg (see STAR Methods), Wg and Aspr showed no colocalization (Figure 8T). However,

upon damage Wg now clearly associates with Aspr-positive EVs at the apical surface (Figure 8U), supporting a model in which Aspr regulates WNT signaling by apically sequestering the Wg ligand during tissue repair.

Thus, our data support a model in which Aspr regulates the timing of Wg signaling targets by modulating Wg ligand availability (Figure 9). Upon damage, *aspr* is initially expressed via its DRMS enhancer in blastema cells alongside *wg* and other secreted factors. During these early regeneration stages, Aspr may facilitate Wg trafficking to promote balanced compartment growth via *vg*, while restraining activation of late patterning genes such as *bs* and *ac*. After 24 h, Aspr levels decline, allowing Wg signaling to reinitiate differentiation programs to promote proper repatterning. Artificially maintaining Aspr beyond this window sequesters Wg apically in EVs, disrupting growth balance and repatterning, resulting in poor regeneration and the characteristic “box wing” phenotype. Conversely, *aspr* knockdown causes premature target activation, further disrupting the precise regenerative sequence required for full wing restoration.

Discussion

Aspr regulates regenerative WNT signaling

Regeneration reactivates developmental programs, yet it often must occur within mature tissues, which poses unique challenges. Temporal coordination is particularly important, as fate specification must follow tissue regrowth to ensure proper repatterning[1,60]. Our findings identify *aspr* as a regeneration-specific gene that accomplishes this by attenuating Wg signaling during early regeneration. *aspr* appears dispensable during development but is activated by damage-induced JNK signaling via a DRMS enhancer,[61] where it functions to properly time WNT-dependent patterning genes in regenerating tissue, potentially via sequestration of the Wg ligand in apically secreted extracellular EVs. This mechanism differs from previously described temporal regulators of regeneration, such as Ets21C and Brat, which act at the level of transcription and translation.[31,62] By contrast, Aspr modulates ligand availability, demonstrating an alternative strategy by which the sequential steps of a regeneration program are maintained. We find that artificially maintaining Aspr disrupts this timing, delaying the restoration of WNT target genes, and leading to defective patterning and disproportional growth. These effects are rescued by pathway activation downstream of the receptor, supporting a model in which Aspr functions at or above the level of WNT

ligand/receptor interaction to negatively regulate Wg signaling during early regeneration. It therefore joins factors such as Evi/Wntless,[51] Porcupine[63,64], SWIM[65], and the heparan sulfate proteoglycans Dally and Dally-like[66], which regulate Wg signaling by controlling overall ligand availability during disc development.[56] Thus, exploring how these factors function in the context of regeneration represents an important direction for future research. Aspr is unlikely to completely block Wg signaling, as some downstream targets, like Dll, remain unaffected with persistent Aspr. Rather, Aspr may fine-tune Wg signaling following injury. Its ability to antagonize WNT activity when co-expressed with activated pathway components, even in undamaged discs (Figure S8P-S8R), suggests it may buffer excess signaling, which is particularly important in regenerative contexts in which signaling is inherently more variable. Interestingly, the effects of maintaining *aspr* expression are more impactful in the anterior compartment. Ectopic Aspr preferentially disrupts anterior patterning, growth, and cell fate markers, and anterior proliferation is more sensitive to its expression. While it is broadly induced in the pouch during wounding, this compartment-specific effect may reflect intrinsic differences in signaling dynamics, proliferation rates, or the influence of anterior-specific regulators. The elevated PCNA activity and delayed vg^{QE} activation in the anterior support this idea. These findings highlight the need to better understand how tissue architecture and compartmental identity influence regenerative signaling. Although compartment-specific identity genes are thought to be largely maintained or quickly reestablished during regeneration,[62,67-69] further studies are needed to understand how A/P compartment identity influences regenerative outcomes.

EV-based control over regenerative timing

During development of the wing disc, Wg is secreted apically and trafficked to the basolateral membrane for receptor interaction.[26,56,58,70-72] Our results suggest that in regeneration, Aspr delays this process by associating with Wg in vesicles that remain apical and separate from the signaling-competent basolateral domains. This may block WNT signaling by physically preventing ligand-receptor interaction, consistent with findings that altering Wg ligand internalization can block signaling.[56,73-75] Once *aspr* expression declines after 24 hours, Wg becomes available for signaling, initiating cell fate specification at the appropriate time. Alternatively, Aspr may alter the secretion or modification of Wg to alter its ability to signal in other ways, since alternative trafficking is known to alter secretion rates, location and post-translational modifications of ligands.[56] Nevertheless, this EV-based mechanism raises

several questions. Is Wg encapsulation actively regulated, or a passive consequence of altered trafficking? What is the fate of Aspr vesicles? Do they carry other morphogens, such as Dpp, or regulatory factors involved in regeneration? The suppression of Dpp target *al* by ectopic Aspr (Figure 6L-N), and the known crosstalk between Wg and Dpp,[76-78] suggests broader regulatory functions that remain to be explored. The localization of Wg to Aspr-containing vesicles during regeneration and not development suggests that additional injury-induced factors may mediate cargo trafficking into these EVs. Given that both Wg and Aspr are regulated by DRMS enhancers,[22] and are co-expressed in “secretory zone” cells of the blastema,[31] it is possible that other factors involved in EV formation or cargo selection are similarly regulated. Therefore, systematic identification of DRMS enhancer targets may uncover additional components or cargoes of EVs that help coordinate regeneration through this mechanism.

Broader implications and future perspectives

This work identifies *aspr* as a novel regeneration-specific gene that regulates tissue patterning by modulating WNT ligand availability via vesicle-based sequestration. These findings underscore the importance of temporal control mechanisms in regeneration and highlight vesicle trafficking as an underexplored mode of signal regulation. Beyond *Drosophila*, EV-mediated intercellular communication is increasingly recognized as critical in cancer and immune biology.[79-82] Our findings suggest that analogous mechanisms may exist in injury and regeneration contexts, and could be harnessed to enhance tissue repair. Future work should focus on the molecular determinants of Wg loading into Aspr vesicles, the identity of additional vesicle cargo, and whether other DRMS-induced genes in blastema cells are regulated via similar mechanisms. Exploring whether vertebrate functional homologs of *aspr* exist, and whether they influence WNT signaling during injury, may open new avenues for regenerative therapies. Ultimately, understanding how tissues control not just which genes are expressed, but also when they are activated, may be essential to unlock the full potential of regenerative biology.

Data and Reagent Availability

All primary data supporting these findings are included within the manuscript or in the supplemental materials. Fly lines generated or used in this work are available upon request; further details regarding stock genotypes are also provided in the Supplementary Genotypes file. For more detailed protocols, please contact the first author, and any further information required to reproduce the experiments can be obtained by contacting the corresponding author.

Acknowledgements

The authors would like to thank Dr. Iswar Hariharan and Dr. David Bilder of UC Berkeley, Dr. Mirka Uhlirova of the University of Cologne, Dr. Seth Bliar of the University of Wisconsin, Dr. Kirsten Guss of Dickinson College, Dr. Baotong Xie of Oregon Health & Science University, Dr. Brian Gebelein of Cincinnati's Children's, Dr. Sonsoles Campuzano of the Centro de Biología Molecular Severo Ochoa, Dr. Gerard Campbell of the University of Pittsburgh for stocks and reagents. Current and former members of the Harris lab for feedback, and the Bloomington Stock Center, Molecular Instruments, and Developmental Studies Hybridoma Bank for stocks and reagents. This research has received no external funding.

Conflicts of Interest

Authors declare no conflicts of interest.

Author Contributions

Si Cave, Conceptualization, Methodology, Investigation Data Curation, Formal Analysis, Validation, Writing – Original Draft, Writing – Review and Editing, Visualization; Manashi Sonowal, Conceptualization, Investigation Data Curation, Formal Analysis, Validation, Writing – Original Draft, Chloe Van Hazel, Investigation Data Curation, Validation, Resources; Petra Fromme, Supervision, Conceptualization, Resources, Robin Harris, Supervision, Conceptualization, Methodology, Investigation Data Curation, Formal Analysis, Funding Acquisition, Writing – Original Draft, Writing – Review and Editing, Visualization, Project Administration.

References

1. Poss, K.D., and Tanaka, E.M. (2024). Hallmarks of regeneration. Cell Stem Cell. 10.1016/j.stem.2024.07.007.
2. Li, Q., Yang, H., and Zhong, T.P. (2015). Regeneration across metazoan phylogeny: lessons from model organisms. J Genet Genomics *42*, 57-70. 10.1016/j.jgg.2014.12.002.
3. Mehta, A.S., and Singh, A. (2019). Insights into regeneration tool box: An animal model approach. Dev Biol *453*, 111-129. 10.1016/j.ydbio.2019.04.006.
4. Walczynska, K.S., Zhu, L., and Liang, Y. (2023). Insights into the role of the Wnt signaling pathway in the regeneration of animal model systems. Int J Dev Biol *67*, 65-78. 10.1387/ijdb.220144yl.
5. Wehner, D., Cizelsky, W., Vasudevaro, M.D., Ozhan, G., Haase, C., Kagermeier-Schenk, B., Roder, A., Dorsky, R.I., Moro, E., Argenton, F., et al. (2014). Wnt/beta-catenin signaling defines organizing centers that orchestrate growth and differentiation of the regenerating zebrafish caudal fin. Cell Rep *6*, 467-481. 10.1016/j.celrep.2013.12.036.
6. Stoick-Cooper, C.L., Weidinger, G., Riehle, K.J., Hubbert, C., Major, M.B., Fausto, N., and Moon, R.T. (2007). Distinct Wnt signaling pathways have opposing roles in appendage regeneration. Development *134*, 479-489. 10.1242/dev.001123.
7. Stewart, S., Gomez, A.W., Armstrong, B.E., Henner, A., and Stankunas, K. (2014). Sequential and opposing activities of Wnt and BMP coordinate zebrafish bone regeneration. Cell Rep *6*, 482-498. 10.1016/j.celrep.2014.01.010.
8. Strand, N.S., Hoi, K.K., Phan, T.M.T., Ray, C.A., Berndt, J.D., and Moon, R.T. (2016). Wnt/beta-catenin signaling promotes regeneration after adult zebrafish spinal cord injury. Biochem Biophys Res Commun *477*, 952-956. 10.1016/j.bbrc.2016.07.006.
9. Wehner, D., Tsarouchas, T.M., Michael, A., Haase, C., Weidinger, G., Reimer, M.M., Becker, T., and Becker, C.G. (2017). Wnt signaling controls pro-regenerative Collagen XII in functional spinal cord regeneration in zebrafish. Nat Commun *8*, 126. 10.1038/s41467-017-00143-0.

10. Perochon, J., Carroll, L.R., and Cordero, J.B. (2018). Wnt Signalling in Intestinal Stem Cells: Lessons from Mice and Flies. Genes (Basel) *9*. 10.3390/genes9030138.

11. Gehart, H., and Clevers, H. (2019). Tales from the crypt: new insights into intestinal stem cells. Nat Rev Gastroenterol Hepatol *16*, 19-34. 10.1038/s41575-018-0081-y.

12. Cordero, J.B., Stefanatos, R.K., Scopelliti, A., Vidal, M., and Sansom, O.J. (2012). Inducible progenitor-derived Wingless regulates adult midgut regeneration in Drosophila. EMBO J *31*, 3901-3917. 10.1038/emboj.2012.248.

13. Tian, A., Benchabane, H., and Ahmed, Y. (2018). Wingless/Wnt Signaling in Intestinal Development, Homeostasis, Regeneration and Tumorigenesis: A Drosophila Perspective. J Dev Biol *6*. 10.3390/jdb6020008.

14. Petersen, C.P. (2023). Wnt signaling in whole-body regeneration. Curr Top Dev Biol *153*, 347-380. 10.1016/bs.ctdb.2023.01.007.

15. De Robertis, E.M. (2010). Wnt signaling in axial patterning and regeneration: lessons from planaria. Sci Signal *3*, pe21. 10.1126/scisignal.3127pe21.

16. Whyte, J.L., Smith, A.A., and Helms, J.A. (2012). Wnt signaling and injury repair. Cold Spring Harb Perspect Biol *4*, a008078. 10.1101/cshperspect.a008078.

17. Tanaka, E.M. (2016). The Molecular and Cellular Choreography of Appendage Regeneration. Cell *165*, 1598-1608. 10.1016/j.cell.2016.05.038.

18. Worley, M.I., and Hariharan, I.K. (2022). Imaginal Disc Regeneration: Something Old, Something New. Cold Spring Harb Perspect Biol *14*. 10.1101/cshperspect.a040733.

19. Tripathi, B.K., and Irvine, K.D. (2022). The wing imaginal disc. Genetics *220*. 10.1093/genetics/iyac020.

20. Fox, D.T., Cohen, E., and Smith-Bolton, R. (2020). Model systems for regeneration: Drosophila. Development *147*. 10.1242/dev.173781.

21. Harris, R.E. (2023). Investigating Tissue Regeneration Using the DUAL Control Genetic Ablation System. Methods Mol Biol *2599*, 255-270. 10.1007/978-1-0716-2847-8_18.

22. Harris, R.E., Stinchfield, M.J., Nystrom, S.L., McKay, D.J., and Hariharan, I.K. (2020). Damage-responsive, maturity-silenced enhancers regulate multiple genes that direct regeneration in Drosophila. Elife *9*. 10.7554/eLife.58305.

23. Klemm, J., Stinchfield, M.J., and Harris, R.E. (2021). Necrosis-induced apoptosis promotes regeneration in Drosophila wing imaginal discs. Genetics *219*. 10.1093/genetics/iyab144.

24. Klemm, J.W., Van Hazel, C., and Harris, R.E. (2025). Regeneration following tissue necrosis is mediated by non-apoptotic caspase activity. Elife *13*. 10.7554/eLife.101114.

25. Quinn, J.W., Lee, M.C., Van Hazel, C., Wilson, M.A., and Harris, R.E. (2024). A threshold level of JNK activates damage-responsive enhancers via JAK/STAT to promote tissue regeneration. bioRxiv, 2024.2010.2031.621241. 10.1101/2024.10.31.621241.

26. Gross, J.C., Chaudhary, V., Bartscherer, K., and Boutros, M. (2012). Active Wnt proteins are secreted on exosomes. Nat Cell Biol *14*, 1036-1045. 10.1038/ncb2574.

27. Mehta, S., Hingole, S., and Chaudhary, V. (2021). The Emerging Mechanisms of Wnt Secretion and Signaling in Development. Front Cell Dev Biol *9*, 714746. 10.3389/fcell.2021.714746.

28. Strigini, M., and Cohen, S.M. (2000). Wingless gradient formation in the Drosophila wing. Curr Biol *10*, 293-300. 10.1016/s0960-9822(00)00378-x.

29. Beckett, K., Monier, S., Palmer, L., Alexandre, C., Green, H., Bonneil, E., Raposo, G., Thibault, P., Le Borgne, R., and Vincent, J.P. (2013). Drosophila S2 cells secrete wingless on exosome-like vesicles but the wingless gradient forms independently of exosomes. Traffic *14*, 82-96. 10.1111/tra.12016.

30. Khan, S.J., Abidi, S.N.F., Skinner, A., Tian, Y., and Smith-Bolton, R.K. (2017). The Drosophila Duox maturation factor is a key component of a positive feedback loop that sustains regeneration signaling. PLoS Genet *13*, e1006937. 10.1371/journal.pgen.1006937.

31. Worley, M.I., Everetts, N.J., Yasutomi, R., Chang, R.J., Saretha, S., Yosef, N., and Hariharan, I.K. (2022). Ets21C sustains a pro-regenerative transcriptional program in blastema cells of Drosophila imaginal discs. Curr Biol *32*, 3350-3364 e3356. 10.1016/j.cub.2022.06.040.

32. Harris, R.E., Setiawan, L., Saul, J., and Hariharan, I.K. (2016). Localized epigenetic silencing of a damage-activated WNT enhancer limits regeneration in mature Drosophila imaginal discs. Elife *5*. 10.7554/eLife.11588.

33. Martin, R., Pinal, N., and Morata, G. (2017). Distinct regenerative potential of trunk and appendages of Drosophila mediated by JNK signalling. Development *144*, 3946-3956. 10.1242/dev.155507.

34. Zeitlinger, J., and Bohmann, D. (1999). Thorax closure in Drosophila: involvement of Fos and the JNK pathway. Development *126*, 3947-3956. 10.1242/dev.126.17.3947.

35. Martin, F.A., and Morata, G. (2006). Compartments and the control of growth in the Drosophila wing imaginal disc. Development *133*, 4421-4426. 10.1242/dev.02618.

36. Wells, B.S., Yoshida, E., and Johnston, L.A. (2006). Compensatory proliferation in Drosophila imaginal discs requires Dronc-dependent p53 activity. Curr Biol *16*, 1606-1615. 10.1016/j.cub.2006.07.046.

37. Huh, J.R., Guo, M., and Hay, B.A. (2004). Compensatory proliferation induced by cell death in the Drosophila wing disc requires activity of the apical cell death caspase Dronc in a nonapoptotic role. Curr Biol *14*, 1262-1266. 10.1016/j.cub.2004.06.015.

38. Zecca, M., and Struhl, G. (2007). Control of Drosophila wing growth by the vestigial quadrant enhancer. Development *134*, 3011-3020. 10.1242/dev.006445.

39. Bray, S. (1999). Drosophila development: Scalloped and Vestigial take wing. Curr Biol *9*, R245-247. 10.1016/s0960-9822(99)80154-7.

40. Kim, J., Sebring, A., Esch, J.J., Kraus, M.E., Vorwerk, K., Magee, J., and Carroll, S.B. (1996). Integration of positional signals and regulation of wing formation and identity by Drosophila vestigial gene. Nature *382*, 133-138. 10.1038/382133a0.

41. Klein, T., and Arias, A.M. (1999). The vestigial gene product provides a molecular context for the interpretation of signals during the development of the wing in Drosophila. Development *126*, 913-925. 10.1242/dev.126.5.913.

42. Fristrom, D., Gotwals, P., Eaton, S., Kornberg, T.B., Sturtevant, M., Bier, E., and Fristrom, J.W. (1994). Blistered: a gene required for vein/intervein formation in wings of Drosophila. Development *120*, 2661-2671. 10.1242/dev.120.9.2661.

43. Montagne, J., Groppe, J., Guillemin, K., Krasnow, M.A., Gehring, W.J., and Affolter, M. (1996). The Drosophila Serum Response Factor gene is required for the formation of intervein tissue of the wing and is allelic to blistered. Development *122*, 2589-2597. 10.1242/dev.122.9.2589.

44. Couso, J.P., Bishop, S.A., and Martinez Arias, A. (1994). The wingless signalling pathway and the patterning of the wing margin in Drosophila. Development *120*, 621-636. 10.1242/dev.120.3.621.

45. Micchelli, C.A., Rulifson, E.J., and Blair, S.S. (1997). The function and regulation of cut expression on the wing margin of Drosophila: Notch, Wingless and a dominant negative role for Delta and Serrate. Development *124*, 1485-1495. 10.1242/dev.124.8.1485.

46. Campbell, G., and Tomlinson, A. (1998). The roles of the homeobox genes aristaless and Distal-less in patterning the legs and wings of Drosophila. Development *125*, 4483-4493. 10.1242/dev.125.22.4483.

47. Rulifson, E.J., and Blair, S.S. (1995). Notch regulates wingless expression and is not required for reception of the paracrine wingless signal during wing margin neurogenesis in Drosophila. Development *121*, 2813-2824. 10.1242/dev.121.9.2813.

48. Phillips, R.G., and Whittle, J.R. (1993). wingless expression mediates determination of peripheral nervous system elements in late stages of Drosophila wing disc development. Development *118*, 427-438. 10.1242/dev.118.2.427.

49. Wouters, M.A., Rigoutsos, I., Chu, C.K., Feng, L.L., Sparrow, D.B., and Dunwoodie, S.L. (2005). Evolution of distinct EGF domains with specific functions. Protein Sci *14*, 1091-1103. 10.1110/ps.041207005.

50. Droujinine, I.A., Meyer, A.S., Wang, D., Udeshi, N.D., Hu, Y., Rocco, D., McMahon, J.A., Yang, R., Guo, J., Mu, L., et al. (2021). Proteomics of protein trafficking by in vivo tissue-specific labeling. Nat Commun *12*, 2382. 10.1038/s41467-021-22599-x.

51. Banziger, C., Soldini, D., Schutt, C., Zipperlen, P., Hausmann, G., and Basler, K. (2006). Wntless, a conserved membrane protein dedicated to the secretion of Wnt proteins from signaling cells. Cell *125*, 509-522. 10.1016/j.cell.2006.02.049.

52. Panakova, D., Sprong, H., Marois, E., Thiele, C., and Eaton, S. (2005). Lipoprotein particles are required for Hedgehog and Wingless signalling. Nature *435*, 58-65. 10.1038/nature03504.

53. Kornberg, T.B. (2017). Distributing signaling proteins in space and time: the province of cytonemes. Curr Opin Genet Dev *45*, 22-27. 10.1016/j.gde.2017.02.010.

54. Stanganello, E., and Scholpp, S. (2016). Role of cytonemes in Wnt transport. J Cell Sci *129*, 665-672. 10.1242/jcs.182469.

55. Alexandre, C., Baena-Lopez, A., and Vincent, J.P. (2014). Patterning and growth control by membrane-tethered Wingless. Nature *505*, 180-185. 10.1038/nature12879.

56. Alvarez-Rodrigo, I., Willnow, D., and Vincent, J.P. (2023). The logistics of Wnt production and delivery. Curr Top Dev Biol *153*, 1-60. 10.1016/bs.ctdb.2023.01.006.

57. Greco, V., Hannus, M., and Eaton, S. (2001). Argosomes: a potential vehicle for the spread of morphogens through epithelia. Cell *106*, 633-645. 10.1016/s0092-8674(01)00484-6.

58. Yamazaki, Y., Palmer, L., Alexandre, C., Kakugawa, S., Beckett, K., Gaugue, I., Palmer, R.H., and Vincent, J.P. (2016). Godzilla-dependent transcytosis promotes Wingless signalling in Drosophila wing imaginal discs. Nat Cell Biol *18*, 451-457. 10.1038/ncb3325.

59. Brunt, L., and Scholpp, S. (2018). The function of endocytosis in Wnt signaling. Cell Mol Life Sci *75*, 785-795. 10.1007/s00018-017-2654-2.

60. Londono, R., Sun, A.X., Tuan, R.S., and Lozito, T.P. (2018). Tissue Repair and Epimorphic Regeneration: An Overview. Curr Pathobiol Rep *6*, 61-69. 10.1007/s40139-018-0161-2.

61. Harris, R.E. (2022). Regeneration enhancers: a field in development. Am J Physiol Cell Physiol *323*, C1548-C1554. 10.1152/ajpcell.00403.2022.

62. Smith-Bolton, R.K., Worley, M.I., Kanda, H., and Hariharan, I.K. (2009). Regenerative growth in Drosophila imaginal discs is regulated by Wingless and Myc. Dev Cell *16*, 797-809. 10.1016/j.devcel.2009.04.015.

63. Kadowaki, T., Wilder, E., Klingensmith, J., Zachary, K., and Perrimon, N. (1996). The segment polarity gene porcupine encodes a putative multitransmembrane protein involved in Wingless processing. Genes Dev *10*, 3116-3128. 10.1101/gad.10.24.3116.

64. van den Heuvel, M., Harryman-Samos, C., Klingensmith, J., Perrimon, N., and Nusse, R. (1993). Mutations in the segment polarity genes wingless and porcupine impair secretion of the wingless protein. EMBO J *12*, 5293-5302. 10.1002/j.1460-2075.1993.tb06225.x.

65. Mulligan, K.A., Fuerer, C., Ching, W., Fish, M., Willert, K., and Nusse, R. (2012). Secreted Wingless-interacting molecule (Swim) promotes long-range signaling by maintaining Wingless solubility. Proc Natl Acad Sci U S A *109*, 370-377. 10.1073/pnas.1119197109.

66. McGough, I.J., Vecchia, L., Bishop, B., Malinauskas, T., Beckett, K., Joshi, D., O'Reilly, N., Siebold, C., Jones, E.Y., and Vincent, J.P. (2020). Glypicans shield the Wnt lipid moiety to enable signalling at a distance. Nature *585*, 85-90. 10.1038/s41586-020-2498-z.

67. Herrera, S.C., and Morata, G. (2014). Transgressions of compartment boundaries and cell reprogramming during regeneration in Drosophila. Elife *3*, e01831. 10.7554/eLife.01831.

68. Repiso, A., Bergantinos, C., and Serras, F. (2013). Cell fate respecification and cell division orientation drive intercalary regeneration in Drosophila wing discs. Development *140*, 3541-3551. 10.1242/dev.095760.

69. Bergantinos, C., Corominas, M., and Serras, F. (2010). Cell death-induced regeneration in wing imaginal discs requires JNK signalling. Development *137*, 1169-1179. 10.1242/dev.045559.

70. Gallet, A., Staccini-Lavenant, L., and Therond, P.P. (2008). Cellular trafficking of the glypican Dally-like is required for full-strength Hedgehog signaling and wingless transcytosis. Dev Cell *14*, 712-725. 10.1016/j.devcel.2008.03.001.

71. Marois, E., Mahmoud, A., and Eaton, S. (2006). The endocytic pathway and formation of the Wingless morphogen gradient. Development *133*, 307-317. 10.1242/dev.02197.

72. Hemalatha, A., Prabhakara, C., and Mayor, S. (2016). Endocytosis of Wingless via a dynamin-independent pathway is necessary for signaling in Drosophila wing discs. Proc Natl Acad Sci U S A *113*, E6993-E7002. 10.1073/pnas.1610565113.

73. Seto, E.S., and Bellen, H.J. (2006). Internalization is required for proper Wingless signaling in Drosophila melanogaster. J Cell Biol *173*, 95-106. 10.1083/jcb.200510123.

74. Blitzer, J.T., and Nusse, R. (2006). A critical role for endocytosis in Wnt signaling. BMC Cell Biol *7*, 28. 10.1186/1471-2121-7-28.

75. Gagliardi, M., Hernandez, A., McGough, I.J., and Vincent, J.P. (2014). Inhibitors of endocytosis prevent Wnt/Wingless signalling by reducing the level of basal beta-catenin/Armadillo. J Cell Sci *127*, 4918-4926. 10.1242/jcs.155424.

76. Zeng, Y.A., Rahnama, M., Wang, S., Lee, W., and Verheyen, E.M. (2008). Inhibition of Drosophila Wg signaling involves competition between Mad and Armadillo/beta-catenin for dTcf binding. PLoS One *3*, e3893. 10.1371/journal.pone.0003893.

77. Eivers, E., Demagny, H., Choi, R.H., and De Robertis, E.M. (2011). Phosphorylation of Mad controls competition between wingless and BMP signaling. Sci Signal *4*, ra68. 10.1126/scisignal.2002034.

78. Li, Y., Zhang, F., Jiang, N., Liu, T., Shen, J., and Zhang, J. (2020). Decapentaplegic signaling regulates Wingless ligand production and target activation during Drosophila wing development. FEBS Lett *594*, 1176-1186. 10.1002/1873-3468.13713.

79. Buzas, E.I. (2023). The roles of extracellular vesicles in the immune system. Nat Rev Immunol *23*, 236-250. 10.1038/s41577-022-00763-8.

80. Kalluri, R. (2024). The biology and function of extracellular vesicles in immune response and immunity. Immunity *57*, 1752-1768. 10.1016/j.immuni.2024.07.009.

81. Kalluri, R., and McAndrews, K.M. (2023). The role of extracellular vesicles in cancer. Cell *186*, 1610-1626. 10.1016/j.cell.2023.03.010.

82. Becker, A., Thakur, B.K., Weiss, J.M., Kim, H.S., Peinado, H., and Lyden, D. (2016). Extracellular Vesicles in Cancer: Cell-to-Cell Mediators of Metastasis. Cancer Cell *30*, 836-848. 10.1016/j.ccell.2016.10.009.

83. Williams, J.A., Bell, J.B., and Carroll, S.B. (1991). Control of Drosophila wing and haltere development by the nuclear vestigial gene product. Genes Dev 5, 2481-2495. 10.1101/gad.5.12b.2481.

84. Affolter, M., Montagne, J., Walldorf, U., Groppe, J., Kloter, U., LaRosa, M., and Gehring, W.J. (1994). The Drosophila SRF homolog is expressed in a subset of tracheal cells and maps within a genomic region required for tracheal development. Development 120, 743-753. 10.1242/dev.120.4.743.

85. Xie, B., Charlton-Perkins, M., McDonald, E., Gebelein, B., and Cook, T. (2007). Senseless functions as a molecular switch for color photoreceptor differentiation in Drosophila. Development 134, 4243-4253. 10.1242/dev.012781.

86. Campbell, G., Weaver, T., and Tomlinson, A. (1993). Axis specification in the developing Drosophila appendage: the role of wingless, decapentaplegic, and the homeobox gene aristaless. Cell 74, 1113-1123. 10.1016/0092-8674(93)90732-6.

87. Kim, J., Sebring, A., Esch, J.J., Kraus, M.E., Vorwerk, K., Magee, J., and Carroll, S.B. (1996). Integration of positional signals and regulation of wing formation and identity by Drosophila vestigial gene. Nature 382, 133-138. 10.1038/382133a0.

Figure Legends

Figure 1. *aspr* is a damage-responsive gene regulated by a DRMS enhancer

(**A-E**) Time course of *aspr* RNA (magenta) in early L3 discs during apoptotic ablation (DC^{hepCA}) in (B-E). *aspr* is strongly induced by 12 h (arrowhead in B), maintained through 24 h, and reduced by 36 h. Unablated control (DC^{NA}) in (A). *aspr* is expressed in the notum and dorsal hinge (arrowheads). Nuclei marked by DAPI (gray).

(**F-G**) *aspr* RNA in late L3 unablated discs (F) showing similar pattern as early L3, and in ablated discs (G) with weak damage-induced expression.

(**H-J**) Necrotic ablation (DC^{gluR1}) in early L3 induces robust *aspr* at 18 h (H, arrowhead), which diminishes by 36 h (I); expression is weaker in late L3 (J).

(**K, L**) AP-1-RFP (cyan) overlaps with damage-induced *aspr* in DC^{hepCA} ablated discs (L, arrowhead), but not in unablated controls (K, open arrowhead).

(**M, N**) *$DRMS^{aspr}$-GFP* RNA (yellow) and *GFP* RNA (green) show overlap in early L3 ablated discs (M, arrowhead) but weak expression in late L3 (N, open arrowhead). *GFP* RNA is absent in notum (M, open arrowhead).

(**O, O'**) *ptc>RFP* undamaged discs show no developmental expression of the *$DRMS^{aspr}$-GFP* reporter (O); *aspr* is expressed developmentally as in (A), (O').

(**P–Q'**) *ptc>egr* and *ptc>hep^{CA}* ablation show strong early L3 *$DRMS^{aspr}$-GFP* and *asp*r RNA expression (P, P') that diminishes in late L3 (Q, Q'). Dotted outlines indicate the pouch.

(**R**) DC^{hepCA} ablation in *hep* null hemizygous mutants shows reduced *aspr* in the ablated pouch (open arrowhead), but preserved developmental expression (arrowhead).

(**S, T**) *pnr>GFP* marks the expression domain (S); *pnr>JNK^{DN}* does not suppress developmental *aspr* (T).

All scale bars: 50 µm. Genotypes are provided in Supplementary File.

Figure 2. aspr is required for regeneration but dispensable for normal development

(**A, B**) *aspr* RNA expression (magenta) in early L3 discs ablated by DC^{hepCA} and imaged at 18 h AHS. (A) Control disc shows strong aspr expression (arrowhead). (B) Knockdown of *aspr* using *DVE>>aspr*^{RNAi} reduces damage-induced expression (open arrowhead). Nuclei labeled with DAPI (gray).

(**C, D**) Representative adult wing phenotypes following ablation. (C) Knockdown of *aspr* in undamaged discs (DC^{NA}, *DVE>>aspr*^{RNAi}) has no effect. (D) Knockdown of *aspr* during regeneration (DC^{hepCA}, *DVE>>aspr*^{RNAi}) impairs wing recovery.

(**E**) Regeneration scoring of adult wings from three conditions: developmental knockdown (DC^{NA}), early L3 ablation, and late L3 ablation. Wings are scored by extent of tissue loss and plotted by proportion. *aspr* knockdown impairs regeneration at both time points. Sample sizes: DC^{NA}: y^{RNAi} (n = 134), $aspr^{RNAi}$ (n = 132); Early L3: y^{RNAi} (n = 50), $aspr^{RNAi}$ (n = 89); Late L3: y^{RNAi} (n = 97), $aspr^{RNAi}$ (n = 109).

(**F**) Quantification of adult wing area from (E). Knockdown of *aspr* during development does not alter size. Knockdown following ablation significantly reduces wing area. Box plots show median and quartiles. Statistics: one-way ANOVA. Sample sizes: DC^{NA}: y^{RNAi} (n = 39), $aspr^{RNAi}$ (n = 52); Early L3: y^{RNAi} (n = 23), $aspr^{RNAi}$ (n = 19); Late L3: y^{RNAi} (n = 25), $aspr^{RNAi}$ (n = 18). ns = not significant; *p = 0.0266; **p = 0.0013.

(**G, H**) DC^{hepCA}-ablated early L3 discs stained for Mmp1 (cyan) and cleaved DCP-1 (yellow). (G) Control shows normal damage response. (H) *aspr* knockdown does not alter Mmp1 or DCP-1 levels.

(**I, J**) Discs from $aspr^{Mi(MIC)}$ mutant larvae. (I) Homozygous $aspr^{Mi(MIC)}$ disc lacks developmental aspr expression in the notum (open arrowhead). (J) $aspr^{Mi(MIC)}/y$ discs ablated by DC^{hepCA} lack both developmental and damage-induced expression (open arrowheads).

(**K, L**) (K) Wings and (L) thorax from $aspr^{Mi(MIC)}$ adults show no morphological defects, indicating normal development in the absence of *aspr*.

(**M**) Regeneration scoring following DC^{hepCA} ablation in w^{1118} (control) and $aspr^{Mi(MIC)}$/+ heterozygotes. Heterozygotes show reduced regeneration at both early and late L3. Sample sizes: Early L3: w^{1118} (n = 18), $aspr^{Mi(MIC)}$/+ (n = 60); Late L3: w^{1118} (n = 41), $aspr^{Mi(MIC)}$/+ (n = 66).

All scale bars: 50 µm unless indicated. Full genotypes listed in Supplementary Genotypes.

Figure 3. Ectopic Aspr disrupts repatterning during regeneration but not normal development

(**A, B'**) Early L3 developmental (DC^{NA}) discs expressing *aspr-HA* (magenta) with *DVE>>GAL4* (A, A') or *ci-GAL4* (B, B'). Aspr-HA appears in discrete puncta in both expression domains. Zoomed views (A', B') highlight focal accumulation (arrowheads). Discs stained for HA (magenta), Nubbin (cyan, A), or Ci (yellow, B), with DAPI (gray).

(**C, D**) DC^{NA} discs expressing *aspr-HA* with *DVE>>GAL4*. Dpp signaling remains unchanged, as assessed by pMad (cyan, C) and *dpp-lacZ* reporter (cyan, D).

(**E, F**) Expression of *aspr-HA* with *ci-GAL4* does not alter Salm (cyan, E) or Nubbin (cyan, F).

(**G, H**) DC^{NA} discs expressing *aspr-HA* and bearing PCNA-GFP (gray) show no change in proliferation.

(**I, J**) Representative adult wings expressing *aspr-HA* in the pouch (I) or anterior compartment (J) show normal morphology.

(**K**) Quantification of wing area from (I-J) shows no significant change upon *aspr-HA* expression. Statistics: one-way ANOVA; ns = not significant. Sample sizes: males – y^{RNAi} (n = 40), *aspr-HA* (n = 44); females – y^{RNAi} (n = 41), *aspr-HA* (n = 40).

(**L**) Regeneration scoring following DC^{hepCA} ablation at early or late L3 with *DVE>>GAL4* driving *aspr-HA* or y^{RNAi}. *aspr-HA* expression reduces regenerative capacity at both time points. Sample sizes: early L3 – y^{RNAi} (n = 50), *aspr-HA* (n = 81); late L3 – y^{RNAi} (n = 67), *aspr-HA* (n = 133).

(**M**) Regeneration scoring using temporally restricted *aspr-HA* expression with *rn-GAL4, GAL80*^{ts}. Early expression (0-24 h AHS) has no effect, while late expression (>24 h) impairs regeneration. Sample sizes: 0-24 h (n = 39); >24 h (n = 30).

(**N**) Wing size measurements from (L). Ectopic *aspr-HA* reduces wing area in both early and late L3 ablation. Box wing phenotypes are indicated in green; other outcomes in purple. Sample sizes: males – y^{RNAi} (n = 25), *aspr-HA* (n = 57); females – y^{RNAi} (n = 15), *aspr-HA* (n = 52). Statistics: one-way ANOVA; ****p<0.0001.

(**O**) Quantification of the box-wing phenotype from (L). Box-wing occurs in 38% of early L3 *aspr-HA* regenerates, but only 5% in late L3. Sample sizes: early L3 – wild type (n = 81), box wing (n = 50); late L3 – wild type (n = 133), box wing (n = 7).

(**P, Q**) Representative adult wings following early (P) or late (Q) *aspr-HA* expression from (M). Early expression yields wild type wings; late expression produces ablation-like phenotypes. Annotated: I2 (black), longitudinal veins (LVx, blue), A/P crossveins (blue).

(**R, R'**) Representative box wing phenotype from (O), showing disrupted patterning. (R**'**) Zoomed anterior view of (R) highlights specific defects: (1) reduced I2, (2) vein fusion, (3) bristle loss, (4) missing ACV, (5) loss of wing margin (numbered arrowheads).

All scale bars: 50 µm unless noted. Genotypes are listed in Supplementary Genotypes.

Figure 4. Ectopic Aspr has an anterior-specific effect on regeneration

(**A, A′**) Wing measurements from early L3 DC^{hepCA} ablated females expressing *aspr-HA* or y^{RNAi} with *DVE>>GAL4*. (A) Wings with box-wing phenotype (green) from *aspr-HA* expression are significantly smaller than control wings (black). (A′) Anterior and posterior areas are both reduced, with a greater effect in the anterior. Statistics: one-way ANOVA. Sample sizes: y^{RNAi} (n = 23), *aspr-HA* (n = 22). ****p < 0.0001; anterior: ****p < 0.0001; posterior: **p = 0.0040.

(**B, B′**) Adult wings from DC^{hepCA} ablation expressing y^{RNAi} (B) or aspr-HA (B′). Anterior and posterior compartments shaded red and purple, respectively. Intervein regions labeled in black.

(**C**) Quantification of intervein regions I1–I4 from anterior in (A′). I2 and I4 are significantly reduced in *aspr-HA* wings. Sample sizes: I1 – y^{RNAi} (n = 15), *aspr-HA* (n = 12); I2 – y^{RNAi} (n = 20), *aspr-HA* (n = 18); I3 – y^{RNAi} (n = 17), *aspr-HA* (n = 19); I4 – y^{RNAi} (n = 26), *aspr-HA* (n = 16). Statistics: one-way ANOVA. ns = not significant; I1, I3 = ns; I2 = ****p = 0.001; I4 = ***p = 0.001.

(**D, E**) Representative adult wings from early L3 DC^{hepCA} ablation expressing *aspr-HA* in the anterior (D, *ci-GAL4*) or posterior (E, *hh-GAL4*). Anterior *aspr-HA* expression produces multiple patterning defects (numbered arrowheads):

(1) reduced I2, (2) vein fusion, (3) bristle loss and ectopic margin, (4) missing ACV, (5) margin loss. Posterior *aspr-HA* expression reduces wing area without affecting patterning (red arrowhead).

(**F**) Time course of regenerating discs expressing *aspr-HA* (DC^{hepCA}, *DVE>>GAL4*), stained for HA (magenta), Nubbin (cyan), Ci (yellow), and DAPI (gray). Anterior pouch appears consistently smaller from 12-60 h AHS. A/P boundary marked with yellow dotted line.

(**G**) Control time course during development (DC^{NA}) shows no change in anterior pouch size with *aspr-HA*. Staining as in (F).

(**H, I**) Quantification of pouch compartments from (F) and controls. (H) Anterior pouch area (% of total disc) is significantly reduced at 36 h, 48 h, and 60 h AHS. (I) Posterior pouch size remains unchanged. Sample sizes: 24 h – y^{RNAi} (n = 20), *aspr-HA* (n = 18); 36 h – y^{RNAi} (n = 17), *aspr-HA* (n = 19); 48 h – y^{RNAi} (n = 26), *aspr-HA* (n = 16); 60 h – y^{RNAi} (n = 10), *aspr-HA* (n = 13). Statistics: one-way ANOVA. Anterior: 24 h = ns, 36 h = *p = 0.0337, 48 h = ***p = 0.0005, 60 h = ***p = 0.0007. Posterior: all time points = ns.

(**J, J′**) *aspr* RNA expression (magenta) at 24 h AHS in DC^{NA} and DC^{hepCA} discs expressing *aspr-HA*. No difference in transcript levels between conditions.

(**K**) Aspr-HA protein (magenta) at 24 h AHS is reduced in the anterior (open arrowhead) relative to the posterior (arrowhead). Ci marks the anterior and outlines the A/P boundary.

(**L**) DC^{NA} disc bearing *R85E08>GFP* (red) shows that the ablation domain spans both compartments similarly. Ci staining outlines the A/P boundary.

All scale bars = 50 µm unless otherwise noted. Full genotypes listed in Supplementary Genotypes.

Figure 5. Aspr impairs anterior proliferation and Vestigial restoration during regeneration

(**A-B‴**) Time course of *PCNA-GFP* expression in early L3 DC^{hepCA} ablated discs, comparing controls (A-A‴) and discs ectopically expressing *aspr-HA* with *DVE>>GAL4* (B-B‴). In controls, PCNA-GFP is elevated at 24-48 h with slight anterior bias and declines by 60 h. *aspr-HA* discs show overall reduced fluorescence at each timepoint. A/P boundary marked by Ci (yellow, dotted line).

(**C**) Quantification of PCNA-GFP intensity across discs at each timepoint. Control discs maintain anterior bias through 48 h; this is reduced in *aspr-HA* discs and lost by 60 h. Splines are LOWESS of data points scaled to disc width.

(**D**) DC^{NA} disc bearing vg^{QE}*-lacZ* at 36 h shows symmetric Vg (cyan) and LacZ (red) expression across A/P boundary (arrowheads).

(**E-E″**) DC^{hepCA} ablated discs lose anterior and posterior Vg at 36 h (E, open arrowheads), but Vg is restored at 48 h and maintained at 60 h (arrowheads). Non-specific staining in disc folds (bright cyan).

(**F-F′**) DC^{NA} vg^{QE}-lacZ discs show consistent enhancer activity at 36 h and 48 h.

(**G-G′**) DC^{hepCA} ablated vg^{QE}*-lacZ* discs lose anterior enhancer activity at 36 h (G, open arrowhead), which is restored at 48 h (G′, arrowhead).

(**H-H″**) *aspr-HA* discs show persistent loss of anterior Vg expression from 36–60 h post-ablation (open arrowheads). Non-specific signal seen in tissue folds (bright cyan).

(**I-N**) Time course of Blistered (Bs, cyan) in DC^{NA} and DC^{hepCA} discs with y^{RNAi} or *aspr-HA*. In development (I, L), Bs marks intervein regions equally. After ablation, Bs is lost at 36 h (J, K) and restored at 60 h in controls (M) but remains absent in *aspr-HA* discs (N).

(**O-P**) Zoomed view of DC^{NA} disc at 60 h (O) and corresponding wing (P), with I2 intervein, longitudinal veins (LVx), and cross veins (A/P CV) labeled.

(**Q–R**) At 60 h post-ablation, control discs restore anterior Bs and I2 (Q), while *aspr-HA* discs fail to restore Bs or reestablish I2 (R).

(**S**) Quantification of intervein region restoration. Controls (black) show robust restoration across I1-I7; *aspr-HA* (magenta) reduces restoration, especially in anterior regions I2 and I3/4.

All scale bars represent 50 µm unless otherwise indicated. Full genotypes are listed in the Supplementary Genotypes file.

Figure 6. Aspr inhibits restoration of anterior cell fate markers during regeneration

(**A**) Undamaged (DC^{NA}) disc stained for Cut (Ct, cyan) shows expression at the wing margin, including the anterior (arrowhead). A/P boundary marked by Ci (yellow, dotted line), nuclei by DAPI (grey).

(**B-D**) Early L3 DC^{hepCA} ablated discs at 48 h (B) and 60 h (C, D) post-ablation stained for Ct. In controls (GFP, green), anterior Ct is absent at 48 h (B, open arrowhead) and restored at 60 h (C, arrowhead). Ectopic *aspr-HA* expression (magenta) prevents Ct restoration at 60 h (D, open arrowhead).

(**E**) DC^{NA} disc stained for Delta (Dl, cyan) shows expression near the wing margin and veins (arrowhead).

(**F-G**) Dl staining at 60 h post-ablation in control (F) and *aspr-HA* (G) discs. Dl is restored in controls (F, arrowhead) but not in *aspr-HA* discs (G, open arrowhead).

(**H**) DC^{NA} disc stained for Achaete (Ac, cyan) shows anterior margin expression (arrowhead).

(**I-K**) Ac staining at 48 h (I) and 60 h (J, K) post-ablation. In controls, Ac is absent at 48 h (I, open arrowhead) and restored at 60 h (J, arrowhead). Ectopic *aspr-HA* prevents restoration (K, open arrowhead).

(**L**) DC^{NA} disc stained for Aristaless (Al, cyan) and Salm (yellow). Al is restricted to the anterior (arrowhead), while Salm marks a domain near the A/P boundary (red arrowhead).

(**M-N**) Staining for Al and Salm at 60 h post-ablation. Both markers are restored in controls (M, yellow and red arrowheads), while *aspr-HA* blocks Al restoration (N, open arrowhead) but does not affect Salm (N, red arrowhead).

(**O**) Quantification of restoration at 60 h for all markers. Y-axis indicates the percentage of discs with full (cyan), partial (turquoise), or no restoration (dark grey). Ectopic *aspr-HA* reduces restoration of all anterior fate markers. Sample sizes: Ct: Control (n = 28), *Aspr-HA* – Full (n = 23), Partial (n = 18), None (n = 9) Dl: Control – Full (n = 11), None (n = 4); *Aspr-HA* – Full (n = 1), None (n = 16) Ac: Control – Full (n = 47), None (n = 9); *Aspr-HA* – Full (n = 3), None (n = 35) Al: Control – Full (n = 9), Partial (n = 4); *Aspr-HA* – Full (n = 1), Partial (n = 11), None (n = 3)

(**P-Q**) Representative wings from early L3 DC^{hepCA} ablation driving *Ets21C* RNAi alone (P) or together with *aspr-HA* (Q). Knockdown of *Ets21C* disrupts regeneration and causes malformed wings, which is rescued by simultaneous ectopic *aspr-HA* expression.

(**R**) Regeneration scoring from (P-Q), categorizing wings by extent of tissue loss. *Ets21C* knockdown reduces regenerative outcomes, while co-expression of *aspr-HA* restores capacity. Sample sizes: Control (n = 27), *Ets21C*^{RNAi} (n = 44), *Ets21C*^{RNAi} , *aspr-HA* (n = 88),

All scale bars represent 50 µm unless otherwise indicated. Full genotypes are provided in the Supplementary Genotypes file.

Figure 7. Structural and *in vivo* analyses show Aspr Is an extracellular protein

(**A**) AlphaFold-predicted structure of full-length Aspr, color-coded by pLDDT confidence: very high (blue, >90), confident (cyan, 70–90), low (yellow, 50–70), and very low (orange, <50).

(**B**) AlphaFold model highlighting seven predicted EGF domains (magenta) and intervening non-EGF regions (cyan). Inset: EGF domain 1 with predicted disulfide bonds (yellow) and cysteine residues.

(**C**) Heatmap of Aspr signal peptide and subcellular localization predictions from six tools (SignalP, Phobius, TargetP, Protter, TMHMM, DeepLoc). Prediction scores range from low (blue, 0) to high (yellow, 1); grey = no data.
(**D**) (i) Structural alignments of the Aspr signal peptide (cyan) with signal peptides from Dumpy isoform V (*Drosophila*, maroon), NELL2 (human, orange), and EDIL3 (mouse, yellow; human, green). (ii) Sequence alignment showing conserved features (e.g., polarity, hydrophobicity), with residues colored by chemical class: hydrophobic (dark red), mildly hydrophobic (red), polar (blue), moderately polar (purple).

(**E**) RMSD values from structural alignments in (D). Each point represents structural similarity between Aspr and comparison proteins; lower values indicate greater similarity.

(**F**) Western blot of hemolymph fractions from control (w^{1118}) and *ci-GAL4>aspr-HA* larvae, probed with HA and Actin antibodies. HA is detected in whole *aspr-HA* larvae (lane 9) and filtered hemolymph (lane 8), and in the supernatant (lane 5) but not the pellet (lane 4) of hemolymph after ultracentrifugation, consistent with secretion. No HA is detected in control larvae (lanes 2–3, 6–7). Actin is detected in whole larvae and filtrate (lanes 8–9).

(**G-G'**) DC^{NA} discs expressing *aspr-HA* (grey) under *ci-GAL4*. Dlg (red) marks the basolateral membrane; DAPI (blue) labels nuclei. (G) Yellow dotted line indicates cross-section shown in (G'), where Aspr-HA localizes apically in cells coinciding with or above Dlg.

(**H-H''**) DC^{NA} discs expressing *aspr-HA* at 24 h. (H) Surface view shows vesicles; yellow box highlights zoomed region in (H'). Open arrowhead marks area lacking vesicles beyond expression domain. (H'') Cross-section reveals vesicles localize to the apical surface.

(**I-I'**) DC^{hepCA} ablated disc expressing *aspr-HA* at 24 h. (I) Surface view shows increased vesicles, with zoomed region in (I'). Arrowhead indicates small vesicles outside the expression domain.

(**J-J'**) Same genotype as (H) imaged without permeabilization. Aspr-HA vesicles are visible (zoomed in J') without diffuse intracellular cytoplasmic signal, consistent with extracellular localization.

All scale bars represent 50 µm unless otherwise indicated. Full genotypes are provided in the Supplementary Genotypes file.

Figure 8. Aspr attenuates WNT signaling

(**A–E**) Time course of *wg* expression from 18-60 h post-ablation in early L3 DC^{hepCA} discs expressing *aspr-HA* (magenta) under *DVE>>GAL4*. Discs are stained for Wg (cyan), Ci (yellow, marking anterior), and DAPI (grey). Yellow dotted lines mark the A/P boundary. From 18-48 h (A-D), Wg is more apparent in the anterior. This effect is no longer observed at 60 h (E), although Wg patterning becomes distorted by a tissue fold.

(**F–J**) Early L3 DC^{hepCA} ablated discs at 60 h post-ablation stained for Achaete (Ac, cyan) and Ci. Control discs (F) restore Ac expression (arrowhead), while *aspr-HA* blocks Ac restoration (G, open arrowhead). Co-expression of *aspr-HA* with WNT pathway activators Axn^{RNAi} (H), *UAS-dsh* (I), or sgg^{RNAi} (J) restores Ac (arrowheads).

(**K**) Quantification of wing phenotypes from (F-J). Ectopic *aspr-HA* induces a box wing phenotype in 39% of wings. This is rescued by WNT activation: 1.7% with Axn^{RNAi}, 0% with *dsh*, and 9.5% with sgg^{RNAi}. Sample sizes: *DVE>>*y^{RNAi} (n=275), Axn^{RNAi} (n=255), *dsh* (n=122), sgg^{RNAi} (n=146); *DVE>>aspr-HA* with y^{RNAi} (n=243), Axn^{RNAi} (n=119), *dsh* (n=63), sgg^{RNAi} (n=288).

(**L**) Quantification of Ac restoration from (H-J) and comparison with *aspr-HA* alone and control from Figure 6O. Ectopic *aspr-HA* reduces Ac restoration to 8% of discs, whereas co-activation of Wg signaling restores Ac in 81% (*Axn*^{RNAi}) and 100% (*dsh*, *sgg*^{RNAi}). Sample sizes: GFP (n=56), *aspr-HA* (n=38), *aspr-HA*; *Axn*^{RNAi} (n=11), *aspr-HA*; *dsh* (n=3), *aspr-HA*; *sgg*^{RNAi} (n=2).

(**M**) Quantification of regeneration outcomes from experiments in (K), categorized by severity of tissue loss. WNT activation alone produces a distinct "ectopic WNT" phenotype (pink), shown in (O). Co-expression with *aspr-HA* slightly reduces this phenotype.

(**N-O**) Representative adult wing phenotypes. (N) Box wing phenotype from *aspr-HA*. (O) Ectopic WNT phenotype with mis-patterning and extra bristles.

(**P-S**) Early L3 DC^{hepCA} discs at 36 h post-ablation bearing *vg*^{QE}*-lacZ* and expressing RNAi for *aspr* (Q), *Axn* (R), or *sgg* (S) under *DVE>>GAL4*. In controls (P), *lacZ* is absent in the anterior (open arrowhead). All RNAi conditions restore anterior *lacZ* expression (arrowheads).

(**T-U**) Wg (cyan or gray) and Aspr-HA (magenta) colocalization at 60 h post-ablation. In developmental (DC^{NA}) discs (T), Aspr-HA vesicles (arrowheads) do not colocalize with Wg (open arrowheads). After damage (DC^{hepCA}, U), Wg is detected at Aspr-HA vesicles (arrowheads). Yellow dotted box indicates region shown at higher magnification insets.

All scale bars represent 50 µm unless otherwise noted. Full genotypes are provided in the Supplementary Genotypes file.

Figure 9. Functional model of Aspr during regeneration

(**A,B**) Schematic model illustrating the proposed role of Aspr in temporally regulating WNT signaling during regeneration. (A) During the first 24 hours post-injury, dying cells induce blastema formation in adjacent tissue with high JNK activity, which activates DRMS enhancers to drive *aspr* and *wg* expression. Aspr localizes to vesicles that contain Wg, limiting its availability to neighboring cells, keeping WNT target genes repressed including *vestigial* (*vg*), *achaete* (*ac*), and *distalless* (*dll*). (B) After 24 hours, Aspr is no longer present, allowing Wg to bind receptors and activate WNT signaling, leading to the expression of cell fate genes and patterning of regenerating tissue. This delay

ensures WNT-mediated patterning occurs only after sufficient growth, coordinating timing and spatial organization during regeneration.

Figure 1

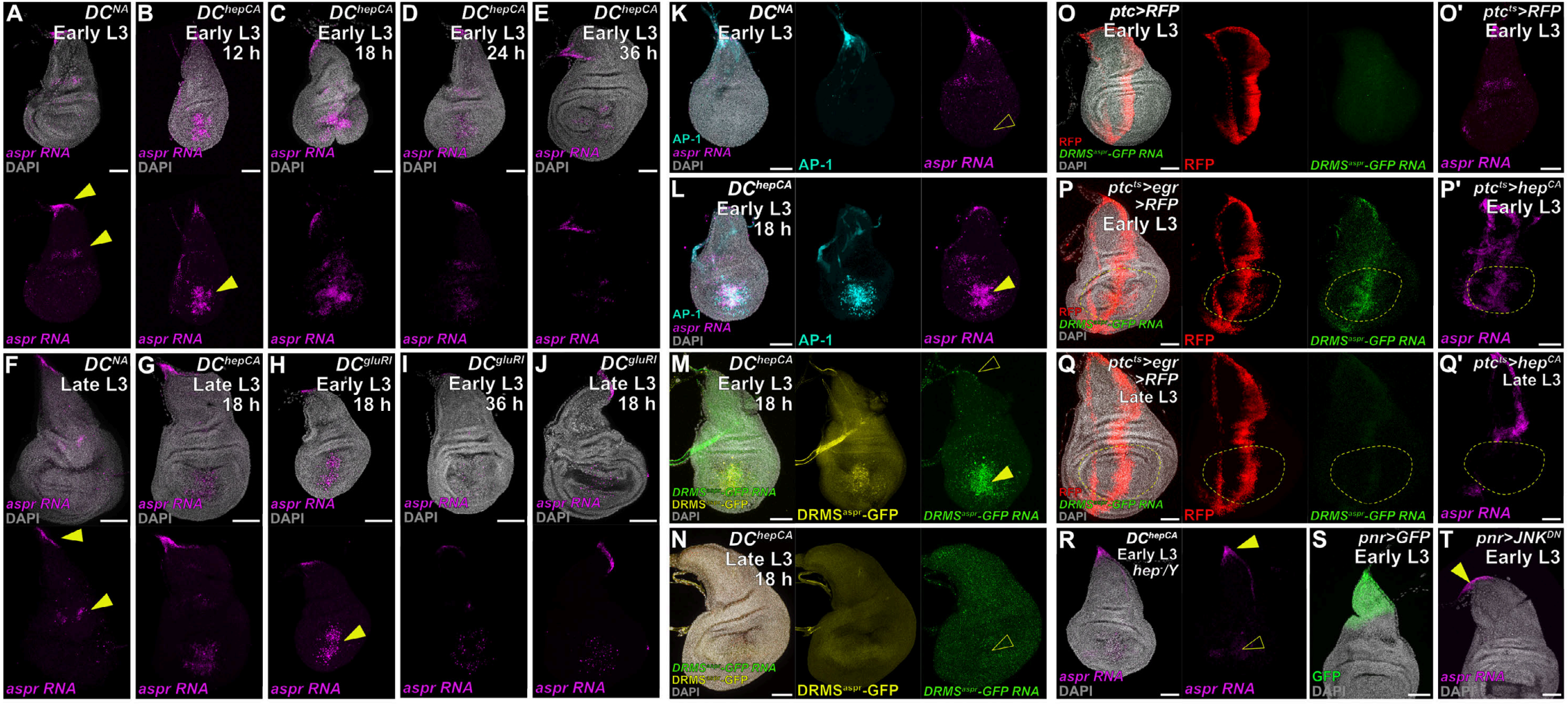
A DC^NA Early L3
B DC^hepCA Early L3 12 h
C DC^hepCA Early L3 18 h
D DC^hepCA Early L3 24 h
E DC^hepCA Early L3 36 h
F DC^NA Late L3
G DC^hepCA Late L3 18 h
H DC^gluRI Early L3 18 h
I DC^gluRI Early L3 36 h
J DC^gluRI Late L3 18 h
K DC^NA Early L3
L DC^hepCA Early L3 18 h
M DC^hepCA Early L3 18 h
N DC^hepCA Late L3 18 h
O ptc>RFP Early L3
O' ptc^ts>RFP Early L3
P ptc^ts>egr >RFP Early L3
P' ptc^ts>hep^CA Early L3
Q ptc^ts>egr >RFP Late L3
Q' ptc^ts>hep^CA Late L3
R DC^hepCA Early L3 hep^-/Y
S pnr>GFP Early L3
T pnr>JNK^DN Early L3
aspr RNA
DAPI
AP-1
RFP
DRMS^aspr-GFP RNA
DRMS^aspr-GFP
GFP

Figure 2

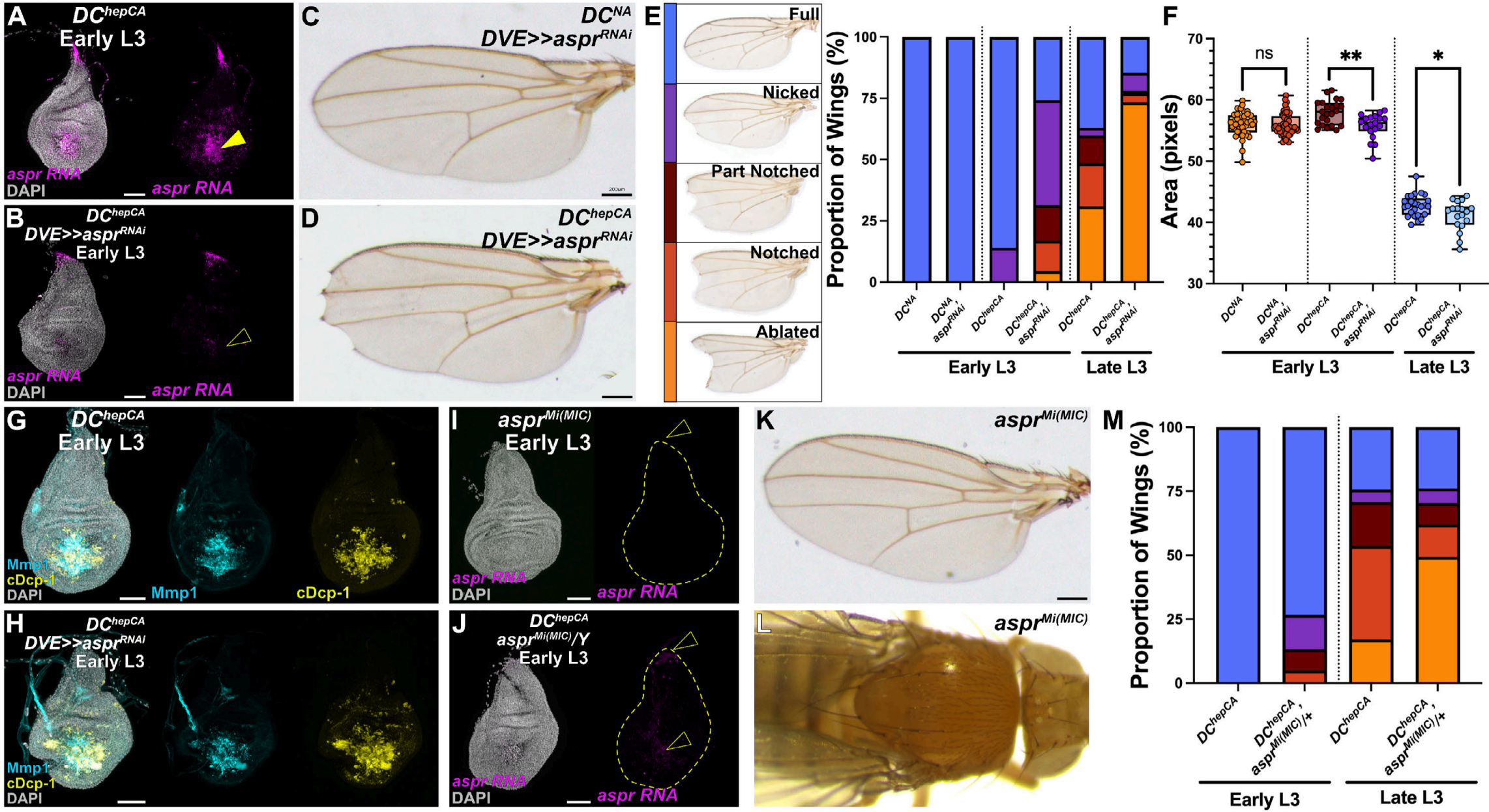
A
DC^hepCA
Early L3
aspr RNA
DAPI
aspr RNA
B
DC^hepCA
DVE>>aspr^RNAi
Early L3
aspr RNA
DAPI
aspr RNA
C
DC^NA
DVE>>aspr^RNAi
D
DC^hepCA
DVE>>aspr^RNAi
E
Full
Nicked
Part Notched
Notched
Ablated
Proportion of Wings (%)
100
75
50
25
0
DC^NA
DC^NA, aspr^RNAi
DC^hepCA
DC^hepCA, aspr^RNAi
DC^hepCA
DC^hepCA, aspr^RNAi
Early L3
Late L3
F
Area (pixels)
70
60
50
40
30
ns
**
*
DC^NA
DC^NA, aspr^RNAi
DC^hepCA
DC^hepCA, aspr^RNAi
DC^hepCA
DC^hepCA, aspr^RNAi
Early L3
Late L3
G
DC^hepCA
Early L3
Mmp1
cDcp-1
DAPI
Mmp1
cDcp-1
H
DC^hepCA
DVE>>aspr^RNAi
Early L3
Mmp1
cDcp-1
DAPI
I
aspr^Mi(MIC)
Early L3
aspr RNA
DAPI
aspr RNA
J
DC^hepCA
aspr^Mi(MIC)/Y
Early L3
aspr RNA
DAPI
aspr RNA
K
aspr^Mi(MIC)
L
aspr^Mi(MIC)
M
Proportion of Wings (%)
100
75
50
25
0
DC^hepCA
DC^hepCA, aspr^Mi(MIC)/+
DC^hepCA
DC^hepCA, aspr^Mi(MIC)/+
Early L3
Late L3

Figure 3

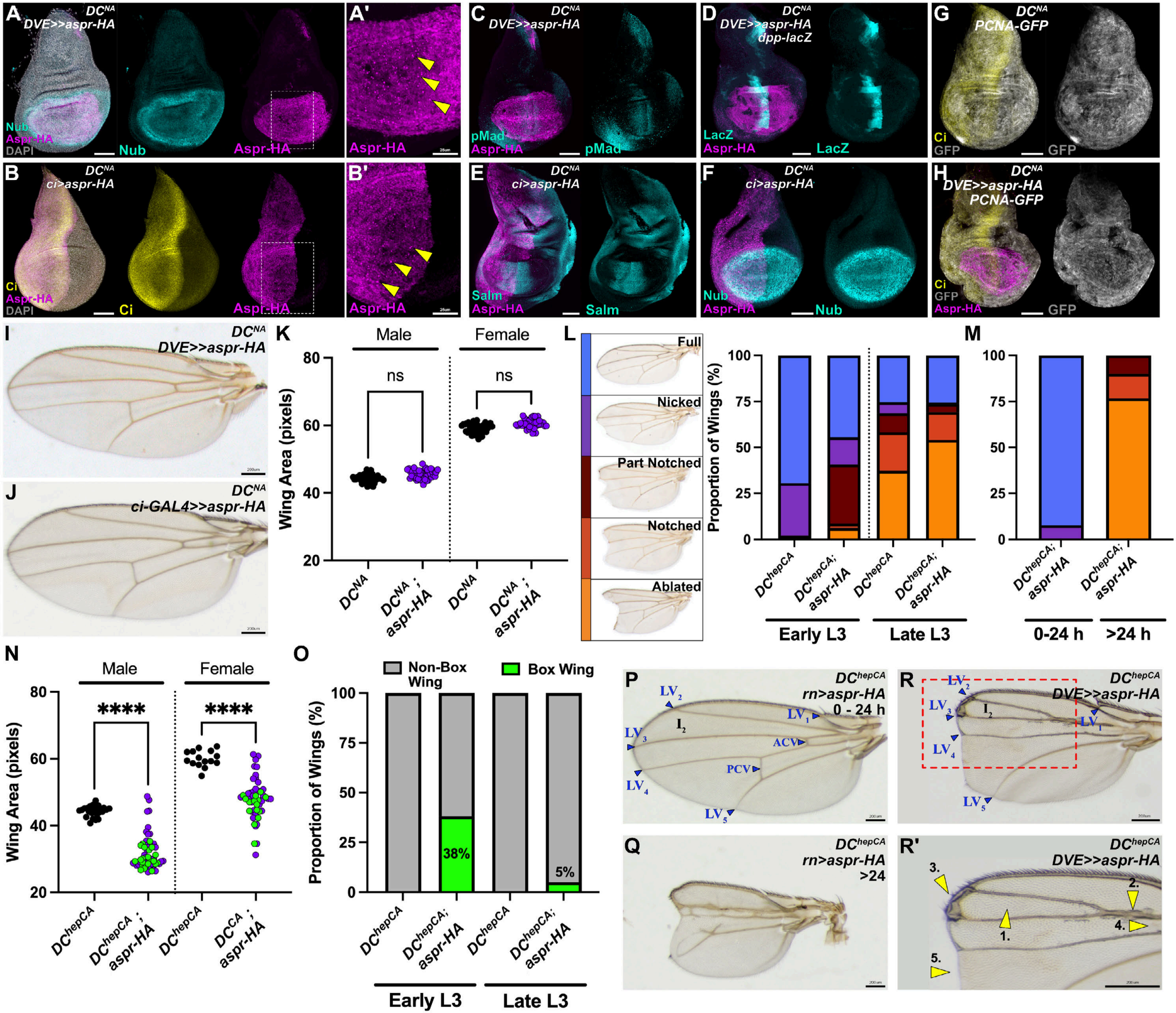
A
DC^NA
DVE>>aspr-HA
Nub
Aspr-HA
DAPI
Nub
Aspr-HA
A'
Aspr-HA
B
DC^NA
ci>aspr-HA
Ci
Aspr-HA
DAPI
Ci
Aspr-HA
B'
Aspr-HA
C
DC^NA
DVE>>aspr-HA
pMad
Aspr-HA
pMad
D
DC^NA
DVE>>aspr-HA
dpp-lacZ
LacZ
Aspr-HA
LacZ
E
DC^NA
ci>aspr-HA
Salm
Aspr-HA
Salm
F
DC^NA
ci>aspr-HA
Nub
Aspr-HA
Nub
G
DC^NA
PCNA-GFP
Ci
GFP
GFP
H
DC^NA
DVE>>aspr-HA
PCNA-GFP
Ci
GFP
Aspr-HA
GFP
I
DC^NA
DVE>>aspr-HA
J
DC^NA
ci-GAL4>>aspr-HA
K
Male
Female
ns
ns
Wing Area (pixels)
80
60
40
20
DC^NA
DC^NA ; aspr-HA
DC^NA
DC^NA ; aspr-HA
L
Full
Nicked
Part Notched
Notched
Ablated
Proportion of Wings (%)
100
75
50
25
0
DC^hepCA
DC^hepCA; aspr-HA
DC^hepCA
DC^hepCA; aspr-HA
Early L3
Late L3
M
100
75
50
25
0
DC^hepCA; aspr-HA
DC^hepCA; aspr-HA
0-24 h
>24 h
N
Male
Female
****
****
Wing Area (pixels)
80
60
40
20
DC^hepCA
DC^hepCA ; aspr-HA
DC^hepCA
DC^CA ; aspr-HA
O
Non-Box Wing
Box Wing
Proportion of Wings (%)
100
75
50
25
0
38%
5%
DC^hepCA
DC^hepCA; aspr-HA
DC^hepCA
DC^hepCA; aspr-HA
Early L3
Late L3
P
DC^hepCA
rn>aspr-HA
0 - 24 h
LV2
LV1
LV3
I2
ACV
PCV
LV4
LV5
R
DC^hepCA
DVE>>aspr-HA
LV2
LV3
I2
LV1
LV4
LV5
Q
DC^hepCA
rn>aspr-HA
>24
R'
DC^hepCA
DVE>>aspr-HA
3.
2.
1.
4.
5.

Figure 4

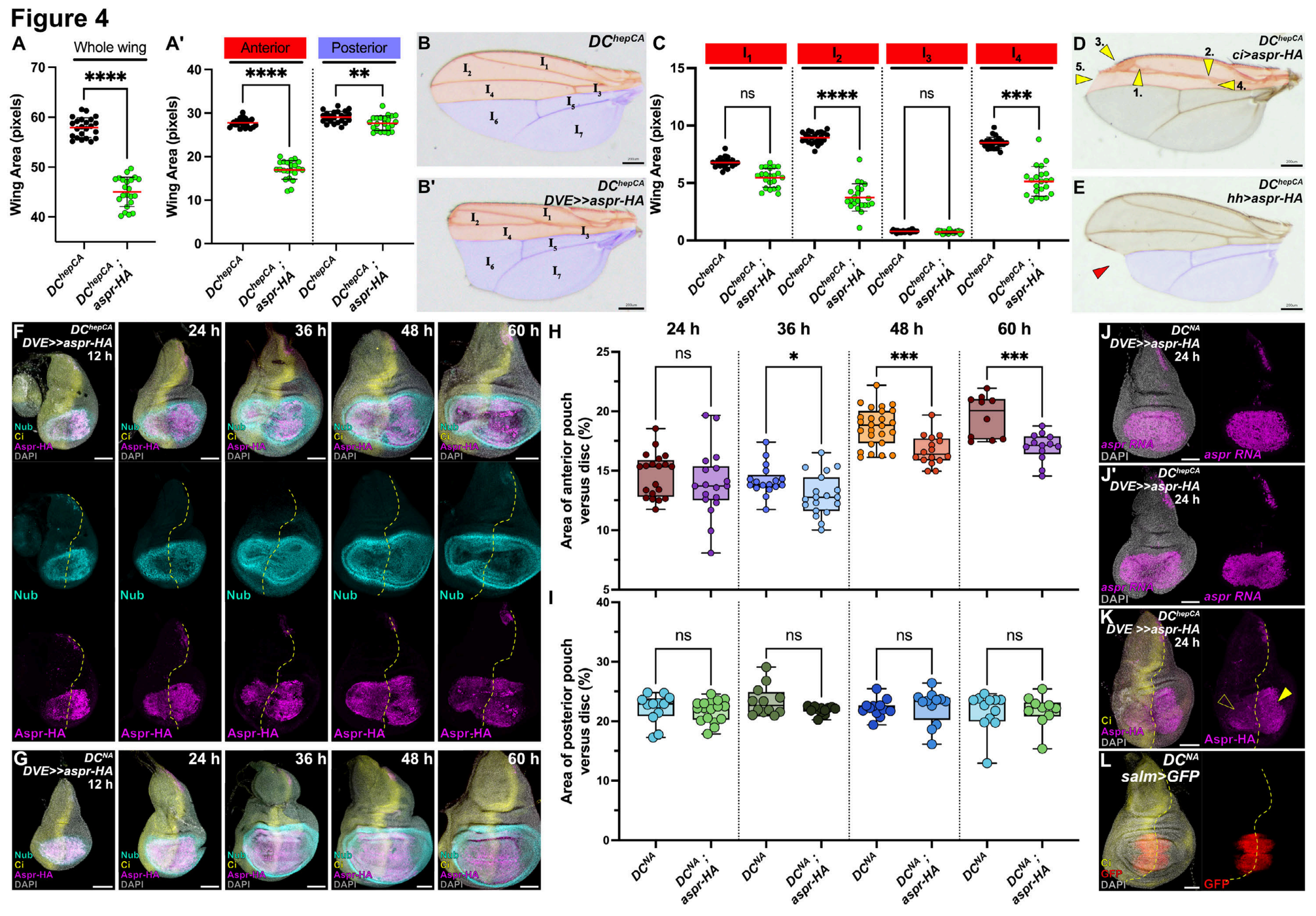
A
Whole wing
Wing Area (pixels)
****
DC^hepCA
DC^hepCA ; aspr-HA
A'
Anterior
Posterior
****
**
B
DC^hepCA
B'
DC^hepCA DVE>>aspr-HA
C
I1
I2
I3
I4
ns
****
ns
***
D
DC^hepCA ci>aspr-HA
E
DC^hepCA hh>aspr-HA
F
DC^hepCA DVE>>aspr-HA 12 h
24 h
36 h
48 h
60 h
Nub
Ci
Aspr-HA
DAPI
G
DC^NA DVE>>aspr-HA 12 h
H
Area of anterior pouch versus disc (%)
*
***
I
Area of posterior pouch versus disc (%)
DC^NA
DC^NA ; aspr-HA
J
DC^NA DVE>>aspr-HA 24 h
aspr RNA
J'
DC^hepCA DVE>>aspr-HA 24 h
K
DC^hepCA DVE >>aspr-HA 24 h
L
DC^NA salm>GFP
GFP

Figure 5

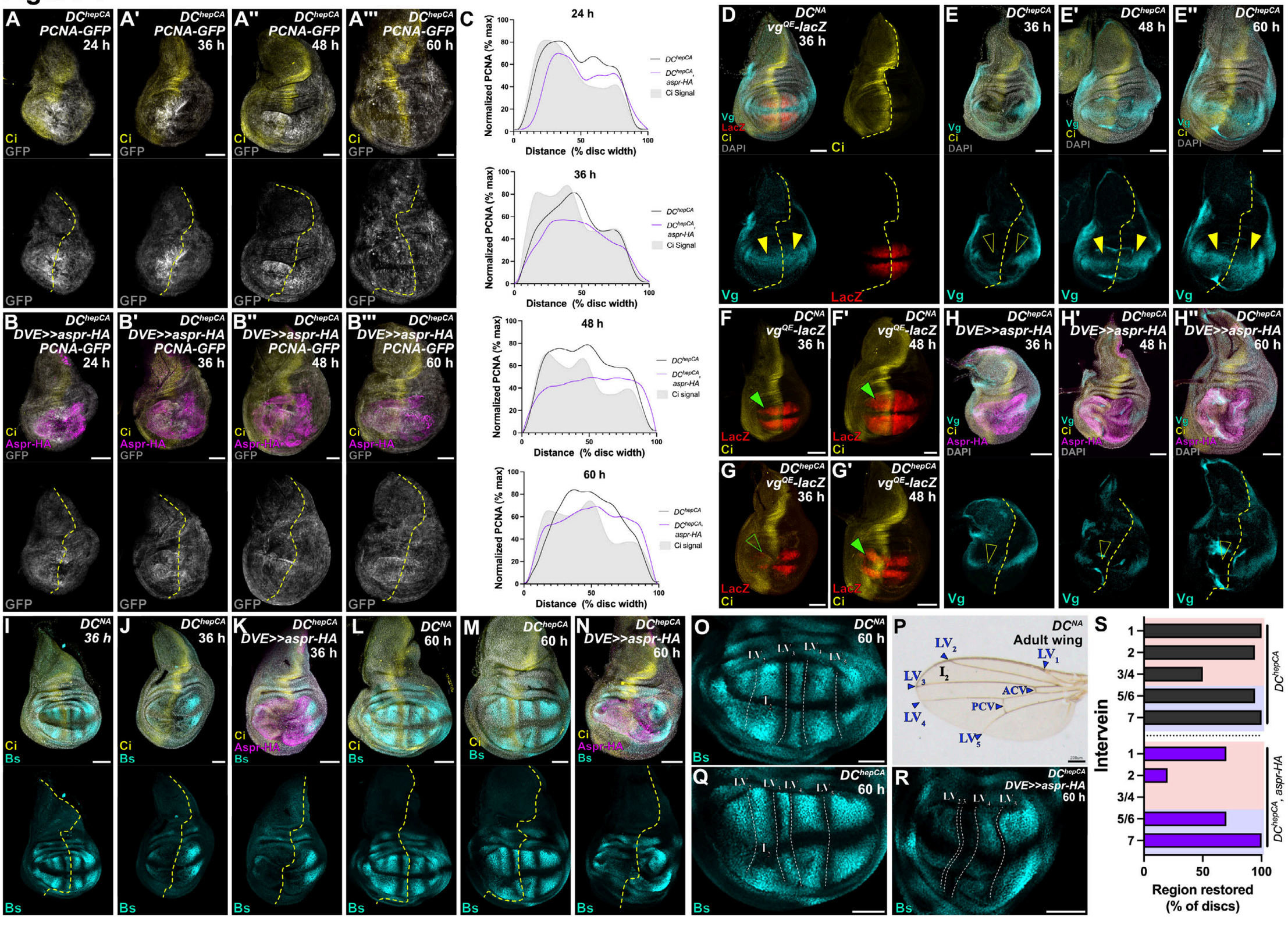
A DC^hepCA PCNA-GFP 24 h
A' DC^hepCA PCNA-GFP 36 h
A'' DC^hepCA PCNA-GFP 48 h
A''' DC^hepCA PCNA-GFP 60 h
Ci
GFP
B DC^hepCA DVE>>aspr-HA PCNA-GFP 24 h
B' DC^hepCA DVE>>aspr-HA PCNA-GFP 36 h
B'' DC^hepCA DVE>>aspr-HA PCNA-GFP 48 h
B''' DC^hepCA DVE>>aspr-HA PCNA-GFP 60 h
Aspr-HA
C
24 h
36 h
48 h
60 h
Normalized PCNA (% max)
Distance (% disc width)
DC^hepCA
DC^hepCA, aspr-HA
Ci Signal
D DC^NA vg^QE-lacZ 36 h
E DC^hepCA 36 h
E' DC^hepCA 48 h
E'' DC^hepCA 60 h
Vg
LacZ
DAPI
F DC^NA vg^QE-lacZ 36 h
F' DC^NA vg^QE-lacZ 48 h
G DC^hepCA vg^QE-lacZ 36 h
G' DC^hepCA vg^QE-lacZ 48 h
H DC^hepCA DVE>>aspr-HA 36 h
H' DC^hepCA DVE>>aspr-HA 48 h
H'' DC^hepCA DVE>>aspr-HA 60 h
I DC^NA 36 h
J DC^hepCA 36 h
K DC^hepCA DVE>>aspr-HA 36 h
L DC^NA 60 h
M DC^hepCA 60 h
N DC^hepCA DVE>>aspr-HA 60 h
Bs
O DC^NA 60 h
P DC^NA Adult wing
LV1
LV2
LV3
LV4
LV5
I2
ACV
PCV
Q DC^hepCA 60 h
R DC^hepCA DVE>>aspr-HA 60 h
S
Intervein
1
2
3/4
5/6
7
DC^hepCA
DC^hepCA, aspr-HA
Region restored (% of discs)

Figure 6

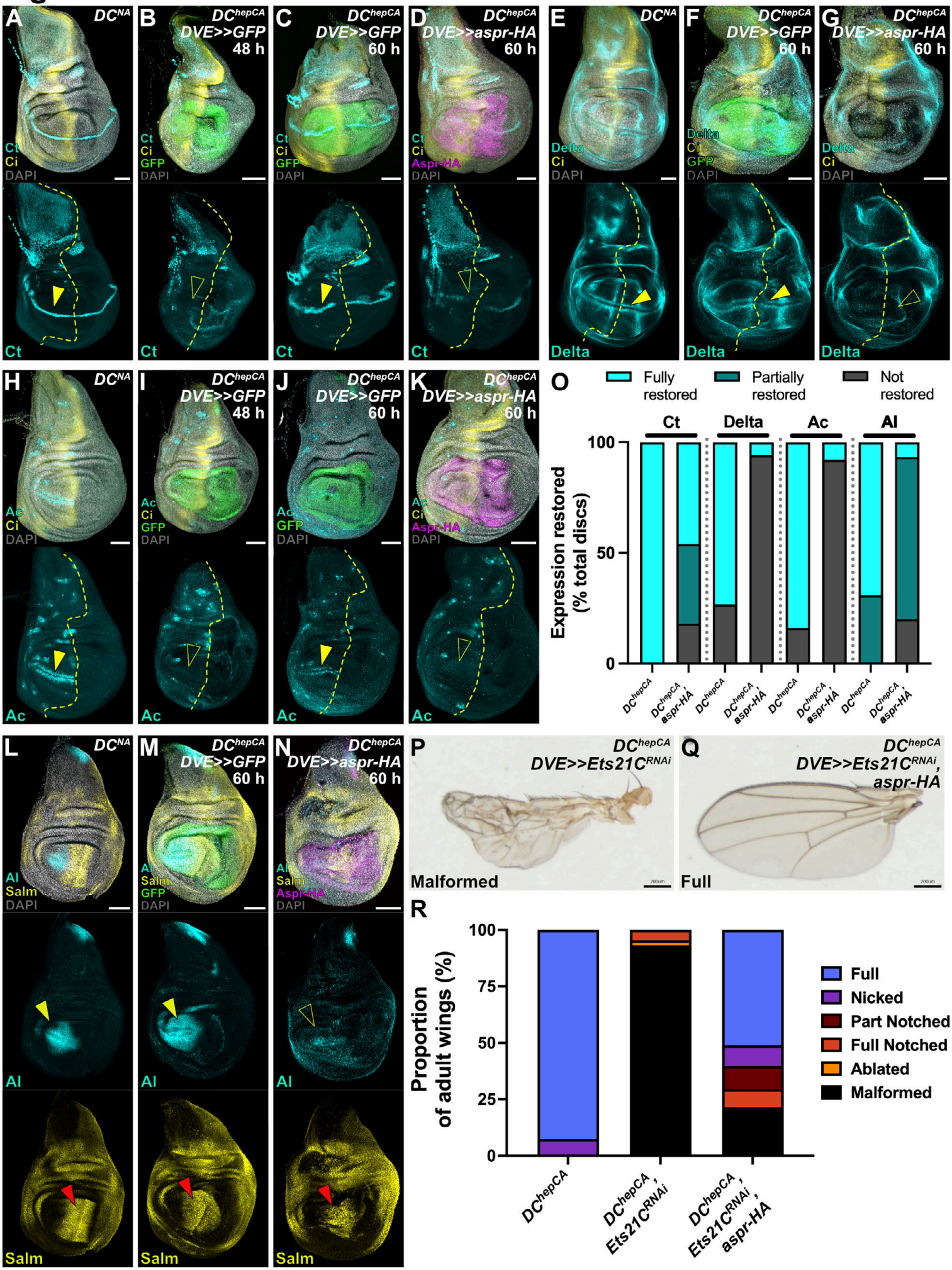
A
DC^NA
Ct
Ci
DAPI
Ct
B
DC^hepCA
DVE>>GFP
48 h
Ct
Ci
GFP
DAPI
Ct
C
DC^hepCA
DVE>>GFP
60 h
Ct
Ci
GFP
DAPI
Ct
D
DC^hepCA
DVE>>aspr-HA
60 h
Ct
Ci
Aspr-HA
DAPI
Ct
E
DC^NA
Delta
Ci
DAPI
Delta
F
DC^hepCA
DVE>>GFP
60 h
Delta
Ci
GFP
DAPI
Delta
G
DC^hepCA
DVE>>aspr-HA
60 h
Delta
Ci
DAPI
Delta
H
DC^NA
Ac
Ci
DAPI
Ac
I
DC^hepCA
DVE>>GFP
48 h
Ac
Ci
GFP
DAPI
Ac
J
DC^hepCA
DVE>>GFP
60 h
Ac
GFP
DAPI
Ac
K
DC^hepCA
DVE>>aspr-HA
60 h
Ac
Ci
Aspr-HA
DAPI
Ac
O
Fully restored
Partially restored
Not restored
Ct
Delta
Ac
Al
Expression restored (% total discs)
100
50
0
DC^hepCA
DC^hepCA, aspr-HA
DC^hepCA
DC^hepCA, aspr-HA
DC^hepCA
DC^hepCA, aspr-HA
DC^hepCA
DC^hepCA, aspr-HA
L
DC^NA
Al
Salm
DAPI
Al
Salm
M
DC^hepCA
DVE>>GFP
60 h
Al
Salm
GFP
DAPI
Al
Salm
N
DC^hepCA
DVE>>aspr-HA
60 h
Al
Salm
Aspr-HA
DAPI
Al
Salm
P
DC^hepCA
DVE>>Ets21C^RNAi
Malformed
Q
DC^hepCA
DVE>>Ets21C^RNAi, aspr-HA
Full
R
Proportion of adult wings (%)
100
75
50
25
0
Full
Nicked
Part Notched
Full Notched
Ablated
Malformed
DC^hepCA
DC^hepCA, Ets21C^RNAi
DC^hepCA, Ets21C^RNAi, aspr-HA

Figure 7

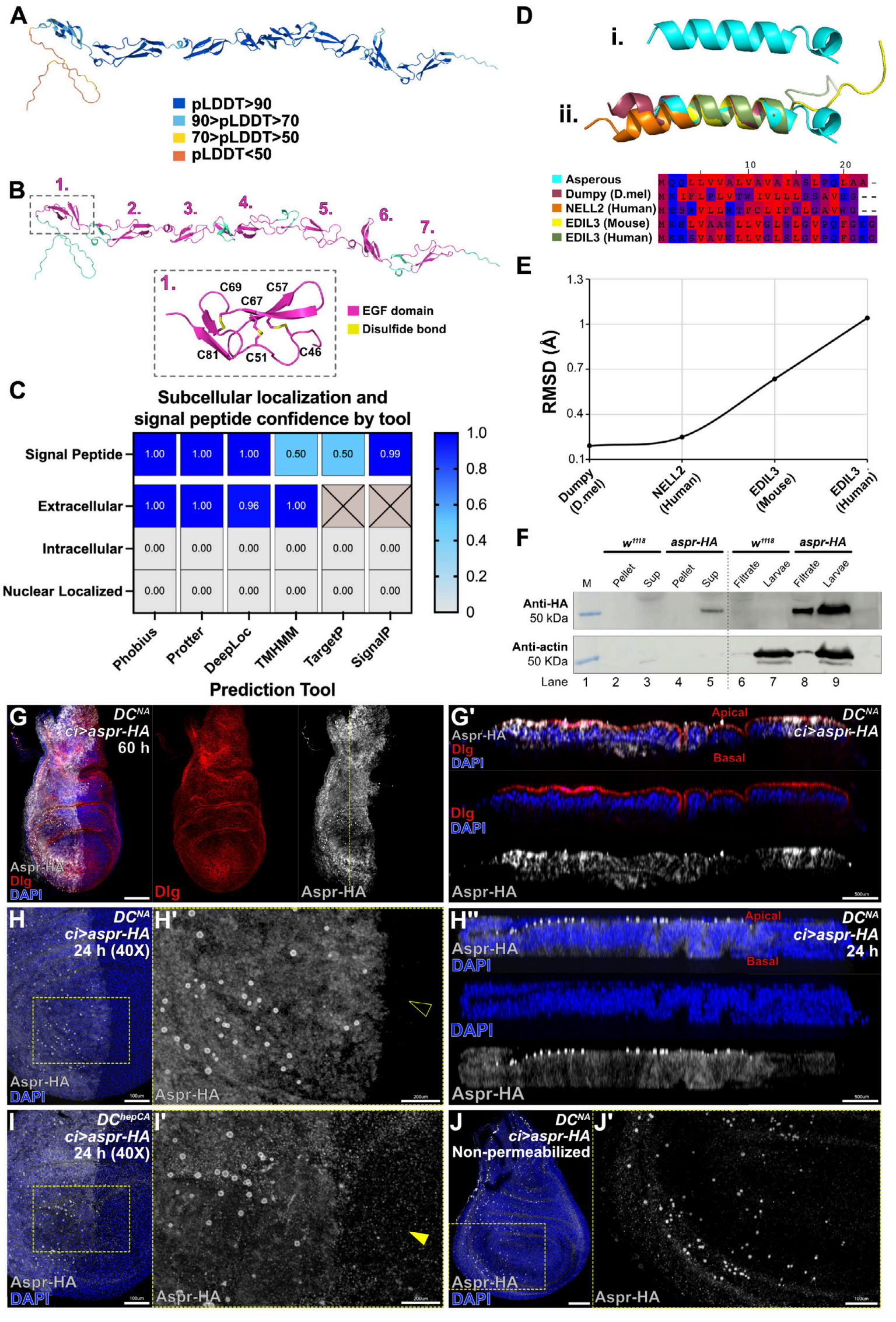
A
pLDDT>90
90>pLDDT>70
70>pLDDT>50
pLDDT<50
B
1.
2.
3.
4.
5.
6.
7.
C69
C57
C67
C81
C51
C46
EGF domain
Disulfide bond
C
Subcellular localization and signal peptide confidence by tool
Signal Peptide
Extracellular
Intracellular
Nuclear Localized
Phobius
Protter
DeepLoc
TMHMM
TargetP
SignalP
Prediction Tool
D
i.
ii.
Asperous
Dumpy (D.mel)
NELL2 (Human)
EDIL3 (Mouse)
EDIL3 (Human)
E
RMSD (Å)
Dumpy (D.mel)
NELL2 (Human)
EDIL3 (Mouse)
EDIL3 (Human)
F
w1118
aspr-HA
Pellet
Sup
Filtrate
Larvae
Anti-HA 50 kDa
Anti-actin 50 KDa
Lane
G
DCNA ci>aspr-HA 60 h
Aspr-HA
Dlg
DAPI
G'
Apical
Basal
H
DCNA ci>aspr-HA 24 h (40X)
H'
H''
DCNA ci>aspr-HA 24 h
I
DChepCA ci>aspr-HA 24 h (40X)
I'
J
DCNA ci>aspr-HA Non-permeabilized
J'

Figure 8

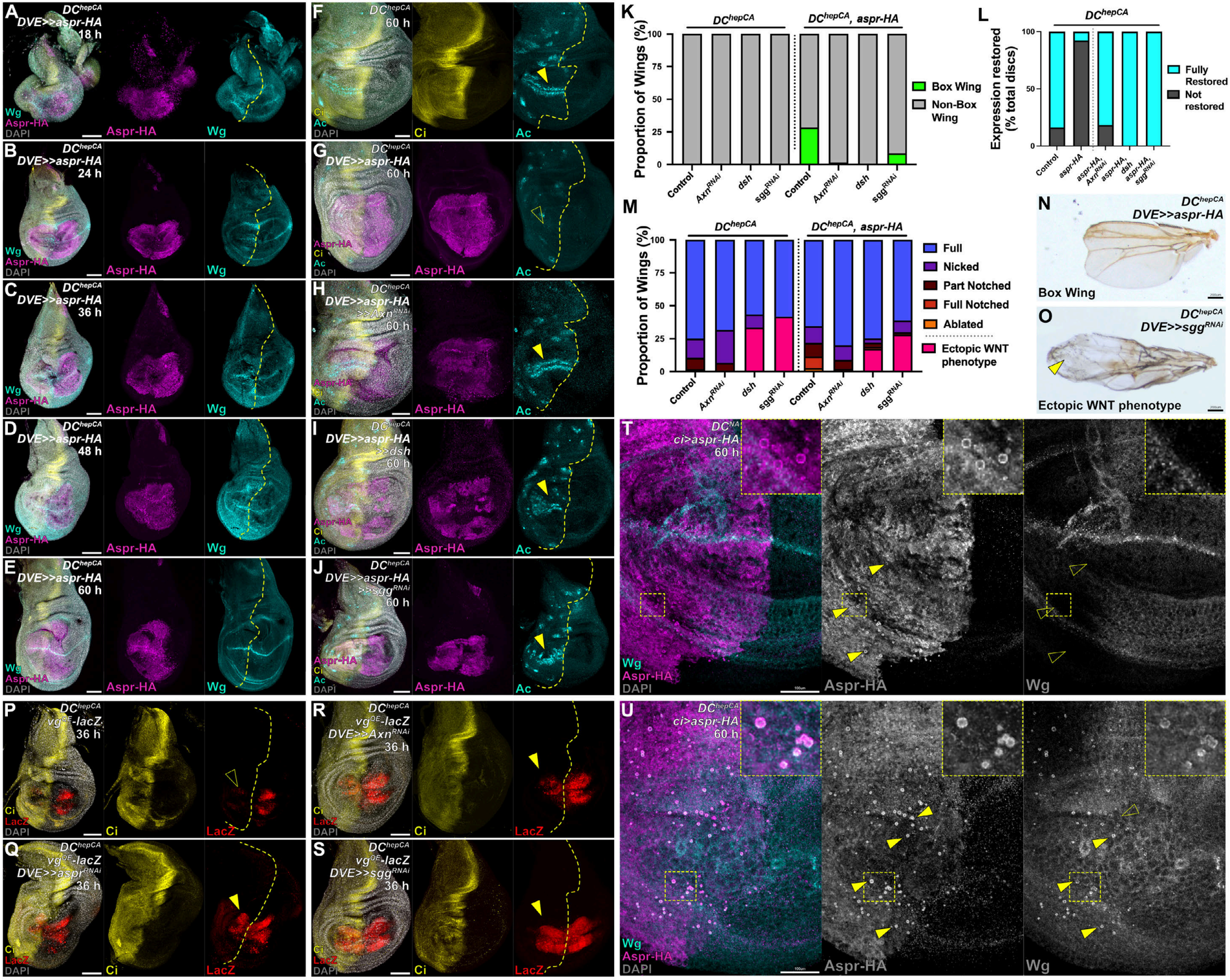
A
DC^hepCA
DVE>>aspr-HA
18 h
Wg
Aspr-HA
DAPI
Aspr-HA
Wg
B
DC^hepCA
DVE>>aspr-HA
24 h
C
DC^hepCA
DVE>>aspr-HA
36 h
D
DC^hepCA
DVE>>aspr-HA
48 h
E
DC^hepCA
DVE>>aspr-HA
60 h
F
DC^hepCA
60 h
Ci
Ac
DAPI
Ci
Ac
G
DC^hepCA
DVE>>aspr-HA
60 h
H
DC^hepCA
DVE>>aspr-HA
>>Axn^RNAi
60 h
I
DC^hepCA
DVE>>aspr-HA
>>dsh
60 h
J
DC^hepCA
DVE>>aspr-HA
>>sgg^RNAi
60 h
K
DC^hepCA
DC^hepCA, aspr-HA
Proportion of Wings (%)
100
75
50
25
0
Control
Axn^RNAi
dsh
sgg^RNAi
Box Wing
Non-Box Wing
L
DC^hepCA
Expression restored (% total discs)
Fully Restored
Not restored
aspr-HA
aspr-HA, Axn^RNAi
aspr-HA, dsh
aspr-HA, sgg^RNAi
M
Full
Nicked
Part Notched
Full Notched
Ablated
Ectopic WNT phenotype
N
DC^hepCA
DVE>>aspr-HA
Box Wing
O
DC^hepCA
DVE>>sgg^RNAi
Ectopic WNT phenotype
P
DC^hepCA
vg^QE-lacZ
36 h
Ci
LacZ
Q
DC^hepCA
vg^QE-lacZ
DVE>>aspr^RNAi
36 h
R
DC^hepCA
vg^QE-lacZ
DVE>>Axn^RNAi
36 h
S
DC^hepCA
vg^QE-lacZ
DVE>>sgg^RNAi
36 h
T
DC^NA
ci>aspr-HA
60 h
U
DC^hepCA
ci>aspr-HA
60 h

Figure 9

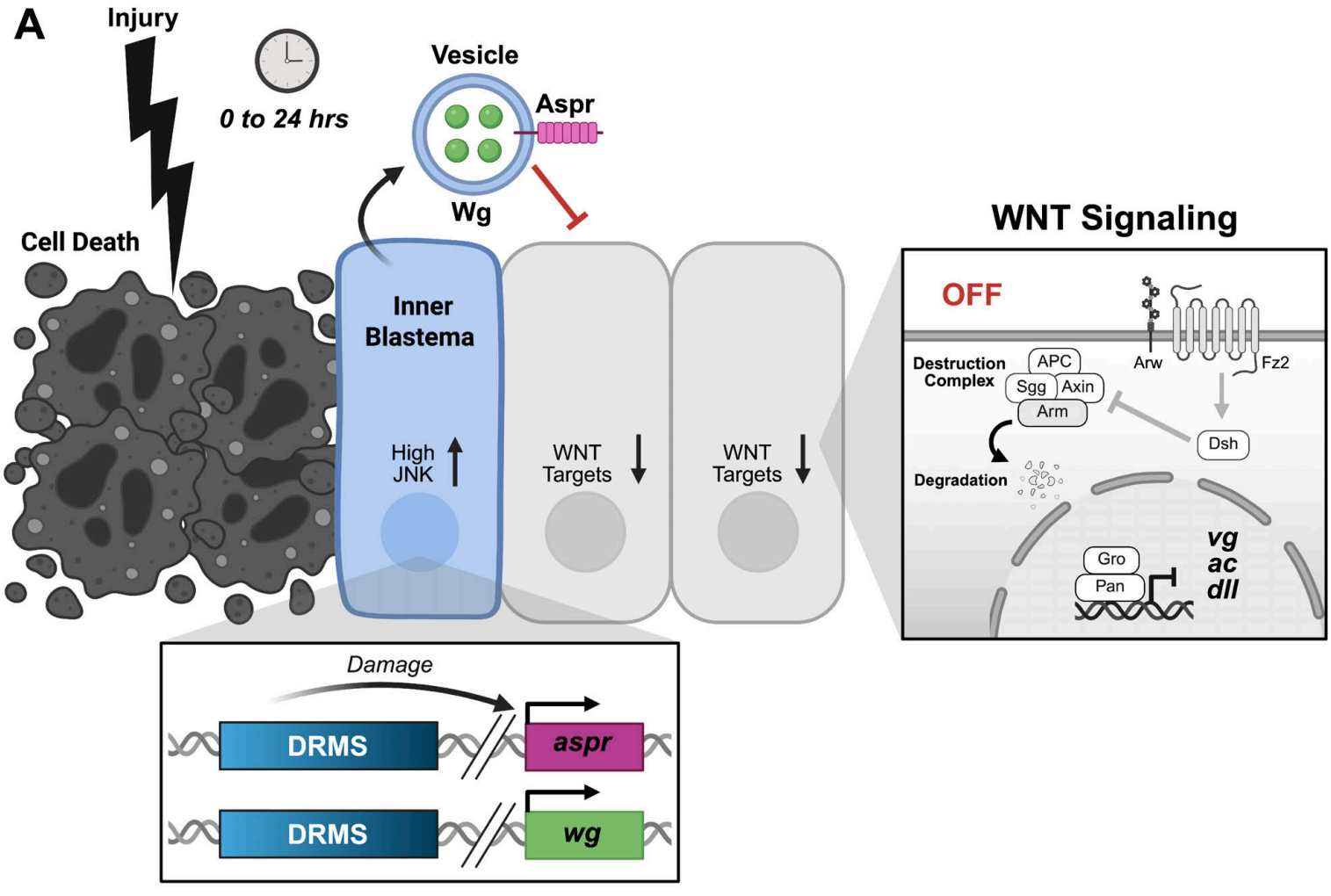
A
Injury
0 to 24 hrs
Vesicle
Aspr
Wg
Cell Death
Inner Blastema
High JNK
WNT Targets
WNT Targets
WNT Signaling
OFF
Destruction Complex
APC
Sgg
Axin
Arm
Arw
Fz2
Dsh
Degradation
Gro
Pan
vg
ac
dll
Damage
DRMS
aspr
DRMS
wg

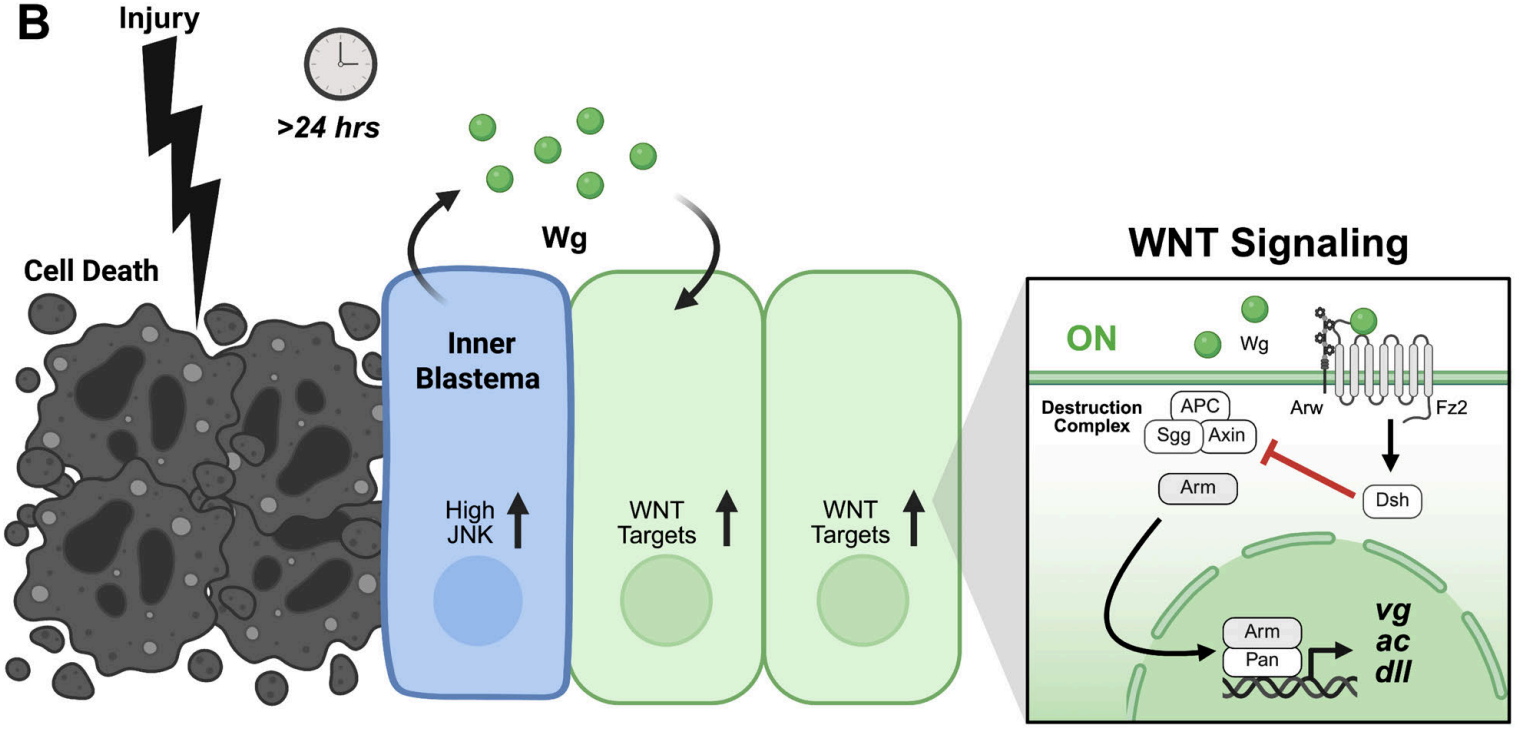
B
Injury
>24 hrs
Wg
Cell Death
Inner Blastema
High JNK
WNT Targets
WNT Targets
WNT Signaling
ON
Wg
Destruction Complex
APC
Sgg
Axin
Arm
Arw
Fz2
Dsh
Arm
Pan
vg
ac
dll